Calhoun: The NPS Institutional Archive
DSpace Repository

Theses and Dissertations 1. Thesis and Dissertation Collection, all items

1958

A Low Power Reactor Simulator

Watkins, James D.

Monterey, California. Naval Postgraduate School

http://hdl.handle.net/10945/7605

Downloaded from NPS Archive: Calhoun

Calhoun is the Naval Postgraduate School's public access digital repository for research materials and institutional publications created by the NPS community. Calhoun is named for Professor of Mathematics Guy K. Calhoun, NPS's first appointed -- and published -- scholarly author.

Dudley Knox Library / Naval Postgraduate School
411 Dyer Road / 1 University Circle
Monterey, California USA 93943

http://www.nps.edu/library

A LOW POWER REACTOR SIMULATOR

James D. Watkins

A LOW POWER REACTOR SIMULATOR

* * * * * * * *

James D. Watkins

A LOW POWER REACTOR SIMULATOR

by

James D. Watkins

Lieutenant, United States Navy

Submitted in partial fulfillment of
the requirements for the degree of

MASTER OF SCIENCE
IN
MECHANICAL ENGINEERING

UNITED STATES NAVAL POSTGRADUATE SCHOOL
Monterey, California

1958

Thesis
W234

A LOW POWER REACTOR SIMULATOR

by

James D. Watkins

This work is accepted as fulfilling
the thesis requirements for the degree of
MASTER OF SCIENCE
IN
MECHANICAL ENGINEERING

from the
United States Naval Postgraduate School

ABSTRACT

Real time simulation of the time-dependent behavior of low power thermal reactors is amenable to analog computer techniques. This paper presents the basic physical concepts relative to thermal reactor operation, a derivation of the governing transient equations noting simplifying assumptions, and the development of the analogous electrical circuit to ultimately provide solutions to these equations. In addition, many special problems involved in the simulation of a specific reactor are discussed and analyzed in detail. As a result, the successful design and construction of a simulator whose time-dependent behavior closely approximates that of an actual reactor is demonstrated. The reactor simulated is the Aerojet-General Nucleonics low power thermal reactor (AGN-201) currently installed at the United States Naval Postgraduate School, Monterey, California. Flux-time recorder plots for various sequences of operation of reactor and simulator are included to indicate the degree of simulation attained.

TABLE OF CONTENTS

Section	Title	Page
1.	Introduction	1
2.	Basic Thermal Reactor Concepts	3
3.	Derivation of the Transient Equations	4
4.	The Electrical Analog	12
5.	Simulation of a Specific Low Power Thermal Reactor AGN 201	18
6.	Degree of Simulation Attained	38
7.	Conclusions	47
8.	Bibliography	48
APPENDIX I	Circuit Analysis Determination of Current, I_8, Corresponding to Rate of Change of Neutron Density With Time	49
APPENDIX II	Scaling Factor Calculations	51

LIST OF ILLUSTRATIONS

Figure		Page
1.	Basic Reactor Simulator Circuit	13
2.	View of Simulated Reactor, AGN-201, Core Tank Assembly	21
3.	Cross-Sectional View AGN-201 Showing Important Features	22
4.	AGN-201 Combined Coarse and Fine Rod Calibration	24
5.	Reactivity Potentiometer Calibration	26
6.	Maximum Reactivity Control and Temperature Coefficient(MRCTC) Potentiometer Schematic	29
7.	Plot of Inhour Equation	31
8.	MRCTC Potentiometer Calibration	32
9.	AGN-201 Electrical Analog Schematic	36
10.	View of the Completed Simulator With Linear Recorder Attached	39
11.	Rear View of Simulator Console Showing All Important Circuit Features	40
12.-14.	Flux-Time Comparison Curves Between Reactor and Simulator For Various Sequences of Operation	42-46

LIST OF ILLUSTRATIONS

Figure		Page
1.	Basic Reactor Simulator Circuit	13
2.	View of Simulated Reactor, AGN-201, Core Tank Assembly	21
3.	Cross-Sectional View AGN-201 Showing Important Features	22
4.	AGN-201 Combined Coarse and Fine Rod Calibration	24
5.	Reactivity Potentiometer Calibration	26
6.	Maximum Reactivity Control and Temperature Coefficient(MRCTC) Potentiometer Schematic	29
7.	Plot of Inhour Equation	31
8.	MRCTC Potentiometer Calibration	32
9.	AGN-201 Electrical Analog Schematic	36
10.	View of the Completed Simulator With Linear Recorder Attached	39
11.	Rear View of Simulator Console Showing All Important Circuit Features	40
12.-14.	Flux-Time Comparison Curves Between Reactor and Simulator For Various Sequences of Operation	42-46

TABLE OF SYMBOLS

n	Thermal neutron population density in neutrons/cm^3
$T^\circ K$	Moderator temperature in $^\circ K$
ϕ	Thermal neutron flux in neutrons/cm^2/sec
v	Mean neutron "speed" in cm/sec
D	Diffusion coefficient in cm
S	Thermal neutron production term in neutrons/cm^3/sec
Σ	Macroscopic cross-section for or probability of occurrence of process denoted by subscripts (a-absorption; l-loss by leakage; f-fission) in cm^{-1}
ν	Total fission yield of fast neutrons (e.g., about 2.5 neutrons per fission of U^{235} nucleus).
β	Total fraction of neutron yield which are delayed ($\beta = \sum_{i=1}^{6} \beta_i$)
β_i	Fraction of neutron yield in i^{th} delayed group
B^2	Buckling in cm^{-2}
τ	Fermi Age in cm^2
p	Resonance escape probability
p_{th}	Thermalization probability ($pe^{-B^2\tau}$)
C_i	Concentration of the i^{th} group of delayed neutron emitters
λ_i	Decay constant for i^{th} delayed neutron precursor in sec^{-1}
ρ	Reactivity ($\rho = \frac{K_{eff} -1}{K_{eff}}$)
K_{eff}	Effective multiplication factor
l^*	Mean neutron lifetime in seconds

l_o^*	Reciprocal neutron thermalization rate or modified neutron lifetime in seconds
T	Stable period in sec (time required to increase power level by a factor of e at a constant value of ρ)

A LOW POWER REACTOR SIMULATOR

1. Introduction.

Detailed analysis of the transient behavior of nuclear reactors has been greatly facilitated by the use of electrical or electronic simulators. A reactor simulator is essentially an analog computer with circuitry specifically designed to solve, on a true time base, the rather complex differential equations governing time-dependent reactor operation.

As will be evident from the development of the governing equations, complete solution by direct analysis would be extremely laborious, if not impossible, for other than a few limited cases where modifying assumptions must be made before a useful solution can be obtained. Moreover, direct mathematical analysis could not be expected to instill in one any real feeling for reactor kinetics under typical operating conditions. Because circuit values can be measured quite precisely, accurate and continuous solutions to the transient equations for almost any imposed operating conditions may be readily obtained from the simulator. In addition, by employing a simple simulator control system, a strong feeling for reactor responses to any of a multitude of typical operating situations may be achieved. This particular feature of the simulator might permit reactor operating personnel or students to receive the equivalent of a great deal of reactor control experience and operational training when access to an actual reactor is not feasible.

Because analog computers are well-tried and accepted engineering tools for use by those involved in the study and design of dynamic systems of all types, reactor simulators find application in preliminary reactor

design and especially in the evaluation and perfection of associated systems which might be ultimately employed to control an actual reactor. In other words, completed control components and systems may be connected to the simulator by means of electronic transducers thereby permitting operational checks to be made on their specific design functions prior to actual installation.

Depending on the complexity of the system to be studied and the degree of simulation desired, simulators may range in size from small units such as the one discussed herein to extremely large, complex, and expensive systems involving the use of great numbers of amplifiers, function generators, servo and electronic multipliers, electro-mechanical devices, and countless precision components. In the case at hand of a particular low power thermal reactor, utilization of the basic simulator circuit together with a relatively simple control network simulates actual reactor operation to a surprisingly good degree of accuracy.

The discussion of basic concepts, the derivation of governing equations and the build-up of the electrical analog represent a compilation of treatments given on this subject by the first seven authors listed in the bibliography. The simulator itself is essentially a Pagels {5}[1] simulator, modified to duplicate more closely the responses of the individual reactor under study.

It must be remembered that the degree of simulation attained can be no better than the degree to which the differential equations utilized define the system under study. The transient equations employed in thermal reactor simulation contain many simplifying assumptions and

[1] Numbers in brackets refer to Bibliography in Section 8.

approximations; and as a consequence, precise duplication of actual reactor behavior may not be expected. Despite these assumptions, however, it will be seen that simulator solutions to the equations employed do closely approximate observed reactor behavior.

It is the purpose of this thesis, therefore, to present a rather complete study in the design of a reactor simulator with the ultimate goal being to construct such a device and then compare time dependent behavior of the actual with that of the analogous system.

2. Basic Thermal Reactor Concepts.

In order that the discussion of the simulation of a low power thermal reactor be complete, it is important that basic concepts be briefly reviewed prior to the derivation of the governing differential equations.

When the nucleus of a fuel atom fissions, it splits into two primary fission fragments of more or less equal mass accompanied by the prompt emission of from two to three neutrons of high energy. On the average, about 2.5 neutrons are liberated per thermal neutron absorbed in fission of a U^{235} nucleus. The majority of these have energies of about one or two Mev. Most of the fission fragments thus formed are radioactive and some are themselves high energy neutron emitters. The decay constants for six delayed neutron precursors have been measured although the precise origin of only three of the six is currently known, namely, BR^{87}, BR^{89}, and I^{137}. The average energy of the delayed neutrons is about .5 Mev. The properties of the delayed neutrons play a vital role in time-dependent reactor behavior and permit safe control of nuclear reactor fission processes which might otherwise be extremely difficult.

In addition to having small thermal neutron absorption cross-sections,

good moderator materials are those made up of elements of low mass number, where the energy transfer from neutron to moderator nucleus on collision may approach 100% as in the case of a hydrogenous moderating medium. This results in extremely rapid slowing down of the high energy neutrons to so-called thermal energies (about .025 ev). At this point, the neutrons are essentially in thermal equilibrium with the moderator atoms (or molecules) and hence are referred to as thermal neutrons. Despite the extremely short slowing down time, some of the neutrons will either escape from the reactor or be absorbed by the core material before thermalization so as to be unavailable for subsequent fissioning or neutron regeneration.

Once the fast neutrons have been reduced to thermal energies, they may leak or diffuse out of the reactor or be absorbed by moderator, fuel, or poison nucleii. A large fraction, about 85%, of the thermal neutrons absorbed by the U^{235} fuel will cause fission; and a new neutron lifetime cycle begins again. The next job, therefore, will be to express in equation form, the lives of neutrons as described above.

3. Derivation of the Transient Equations.

Based on the conservation or balance of neutrons principle, applicable to any reactor, a general expression for the rate of change of neutron population density (n) with time can be written as follows:

$$\text{Production-Absorption-Leakage} = \frac{\delta n}{\delta t} \qquad (1)$$

The rate of production of neutrons may be obtained from empirical considerations. Likewise, the rate of absorption depends on various absorption cross-sections which must be determined experimentally. For determining leakage, resort is made to classical mechanics and the familiar laws of diffusion theory which, although somewhat more complicated, can be

reduced to simplified expressions when certain prudent assumptions are introduced. Let us now form the basis on which the various simplifying assumptions can be made.

The thermal reactor to be considered here is of the homogeneous type with reflector. The fuel is a homogeneous mixture of U^{235} in the form of 20% enriched UO_2 with polyethylene, $(CH_2)_n$, as the moderating material. A thin high density graphite reflector is employed. However, in the analysis which follows, it will be assumed that the reactor is homogeneous but unreflected. The degree to which this assumption is valid can best be appraised by a comparison between final simulator solution and actual time-dependent reactor test runs. As will be seen later, the assumption was quite reasonable in this case.

Before continuing with additional assumptions, it will be helpful to rewrite equation (1) as the familiar diffusion equation for thermal neutrons in non-equilibrium, basic to reactor theory, namely

$$S - \Sigma_a \phi - (-D\nabla^2\phi) = \frac{\delta n}{\delta t} \qquad (2)$$

where S is the production term in neutrons per cm^3 per second, Σ_a is the macroscopic absorption cross-section for monoenergetic (or thermal) neutrons in cm^{-1}, ϕ is the thermal neutron flux in neutrons per cm^2 per sec, and $(-D\nabla^2\phi)$ is the neutron leakage per cm^3 per sec. By the acceptance of equation (2) as the equation representing (1), it has been assumed that we are dealing only with monoenergetic (or thermal) neutrons and then only at distances greater than two or three mean free paths from strong absorbers, sources, or boundaries. This also assumes that the moderating or diffusion medium is a poor absorber relative to its ability to scatter and, hence, slow down the high energy neutrons. The partial derivative of n is utilized because n is a function of both position and time. However, it will be presumed

that the reactor is at or near critical and the shape of the flux distribution remains constant even though it changes in amplitude with time. Under the latter provision, $(-D\nabla^2\phi)$ could be represented by some constant multiplied by the flux ϕ. Making use of this, therefore, let $(-D\nabla^2\phi) = \Sigma_l \phi$, where the symbol Σ will be used throughout this development to indicate the macroscopic cross-section for or the probability of occurrence of the particular process indicated by the subscript, i.e., in this case Σ_l to mean probability of loss by leakage or leakage coefficient. This essentially eliminates the space variable and permits the use of the total derivative of n, or $\frac{dn}{dt}$ in lieu of $\frac{\delta n}{\delta t}$. The flux ϕ under the above considerations is merely the product of n, the density of thermal neutrons in neutrons per cubic centimeter, and v, the mean thermal neutron "speed." Or, expressed in equation form,

$$\phi = nv \quad \text{neutrons } /\text{cm}^2/\text{sec}$$

Thermal neutron flux ϕ, therefore, is a scalar quantity. We are now in a position to examine each of the terms of equation (2) in an attempt to develop a more workable and meaningful equation.

The source term (S) must be broken into several parts, i.e., S_p, S_d, and S_0, referring respectively to prompt, delayed, and those uniformly distributed as a consequence of an extraneous outside source (e.g., a Ra-Be source). Expressed in equation form:

$$S = S_p + S_d + S_0 \tag{3}$$

The rate of fission can be expressed as $\Sigma_f\phi$. If ν represents the total fission yield of fast neutrons from both delayed and prompt sources and β represents the total fraction of these neutrons which are delayed, then

the prompt neutron generation rate is given by

$$\Sigma_f \phi \nu (1-\beta)$$

However, not all of these neutrons reach thermal energies. As previously mentioned some leak out or escape and others may be captured by fuel or other nucleii during the moderating or slowing down process. Probabilities have been evaluated for each of these processes. The former is given by the fast non-leakage probability, $e^{-B^2\tau}$ (where B^2 is the so-called buckling factor related to size and τ is the Fermi Age, a measure of the distance neutrons travel in slowing from fission to thermal energies), and the latter by p, the resonance escape probability. For simplicity, these factors will be combined into a single thermalization probability symbolized by p_{th}. Therefore, the prompt thermal source becomes

$$S_p = \phi \Sigma_f (1-\beta) \nu p_{th} \tag{4}$$

where $p_{th} = pe^{-B^2\tau}$. Now the remainder of the neutrons are the so-called delayed neutrons associated with the particular fission fragments mentioned in section 2. The delayed neutron generation rate, therefore, is given by

$$\Sigma_f \phi \beta \nu$$

Now, as previously stated, six delayed neutron precursors have been determined so that the delayed neutron generation rate of each of the six may be expressed by

$$g_i = \Sigma_f \phi \beta_i$$

where β_i = fraction of total number of neutrons contained in the i^{th}

delayed group. It should be noted here that $\beta = \sum_{i=1}^{6} \beta_i$. At any time, there will be a concentration C_i of the i^{th} group of delayed neutron emitters present in a unit volume of the core. Because these delayed neutrons are emitted as a result of the normal radioactive decay of the precursors, each emitter obeys the familiar radioactive decay law. In other words, the rate of change of the concentration of the i^{th} group will be equal to the production rate minus the decay rate, or

$$\frac{dC_i}{dt} = g_i - \lambda_i C_i$$

where λ_i is the decay constant for the i^{th} emitter.

Therefore,

$$\frac{dC_i}{dt} = \Sigma_f \phi \beta_i \nu - \lambda_i C_i \qquad (5)$$

Delayed neutrons are therefore supplied to the reactor at the same rate at which decay of the precursors takes place. This can be expressed as a summation $\sum_{i=1}^{6} \lambda_i C_i$. Because the average energies of the delayed neutrons are somewhat less than those of the prompt, there will be less tendency for the delayed neutrons to leak out during the slowing down process; and hence they will have larger values of non-leakage probabilities. The difference in the values of non-leakage probability for the two types may be taken into account by utilizing effective values of β_i in the final equations which are slightly larger than the actual values. This, then, permits multiplication of the delayed neutron term by the same value of non-leakage probability as that used for the prompt neutron term. Combining this factor again with the resonance escape probability p,

the rate at which delayed neutrons are supplied can now be expressed as a summation of terms, namely

$$S_d = p_{th} \sum_{i=1}^{6} \lambda_i C_i \tag{6}$$

where $\lambda_i C_i$ is defined by equation (5). Finally, S_0 comes from an essentially constant extraneous source of neutrons which makes a contribution to production rate in the form of a uniformly distributed source. This term will be discussed in more detail later.

The absorption term in equation (2) needs no additional explanation except to say that Σ_a represents the macroscopic absorption cross-section for all processes, that is absorption of thermal neutrons by structure, moderator, fuel, or poison nucleii.

The leakage term was discussed earlier and can be taken to equal $\Sigma_l \phi$, where Σ_l is dependent on the moderator characteristic and reactor size.

The component terms of equation (2) can now be assembled as follows:

$$\frac{dn}{dt} = (S_p + S_d + S_0) - \Sigma_a \phi - \Sigma_l \phi$$

$$\frac{dn}{dt} = \left[\phi \Sigma_f (1 - \beta) \nu p_{th} + p_{th} \sum_{i=1}^{6} \lambda_i C_i + S_0 \right] - \phi (\Sigma_a + \Sigma_l)$$

or $$\frac{dn}{dt} = \left[(\phi \Sigma_f \{1 - \beta\} \nu + \sum_{i=1}^{6} \lambda_i C_i) p_{th} \right] - \phi (\Sigma_a + \Sigma_l) + S_0 \tag{7}$$

In order to reduce equations (5) and (7) to more usable forms, several terms must be defined. First, the term reactivity ρ may be defined as

$$\rho \equiv \frac{K_{eff} - 1}{K_{eff}} \tag{8}$$

where K_{eff} is the effective multiplication factor for a given finite sized reactor. By effective multiplication factor is meant the population ratio of successive neutron generations. If l^* is next defined as the mean lifetime of thermal neutrons in the reactor and $1/l_0^*$ as the rate at which neutrons, prompt and delayed, are thermalized in the reactor, then K_{eff} could also be expressed as the ratio of l^* / l_0^* {6}, or

$$K_{eff} = l^* / l_0^* \tag{9}$$

This may be interpreted as follows: K_{eff} is the ratio of the time spent by the thermal neutrons diffusing in the reactor to the time spent in being thermalized. In other words, if it takes longer to thermalize the second generation of thermal neutrons than the life expectancy of the first generation, the chain can be expected to die out. In this case, K_{eff} would be less than unity. The reverse would be true if K_{eff} were greater than unity. When K_{eff} is precisely unity (or in the case of the presence of an extraneous source, slightly less than unity), just as many thermal neutrons are born as die and the chain is sustained. These three situations represent subcritical, supercritical, and critical behavior of the reactor. l_0^* can be expressed as the reciprocal of the thermalization rate {6}, or

$$l_0^* = \frac{1}{v \Sigma_f \sqrt{\;} p_{th}} \tag{10}$$

This term is also given the name of modified lifetime by Murray {3}. Now thermal neutron lifetime in an infinite medium would be given by the average distance traveled by the neutron before absorption, called the absorption mean free path, $\lambda_a \left(= \frac{1}{\Sigma_a} \right)$, divided by the mean neutron velocity v. However, in a finite reactor, this must be reduced by the

thermal leakage factor

$$\frac{\text{Thermal Absorption}}{\text{Thermal Absorption + Thermal Leakage}}$$

or $$l^* = \frac{1}{v\Sigma_a} \cdot \frac{\Sigma_a}{\Sigma_a + \Sigma_l} = \frac{1}{v(\Sigma_a + \Sigma_l)} \qquad (11)$$

Substituting (9), (10), and (11) into (8), therefore,

$$\rho \equiv 1 - \frac{1}{l^*/l_0^*} = 1 - \frac{v(\Sigma_a + \Sigma_l)}{v\Sigma_f \nu p_{th}} \qquad (12)$$

Now, utilizing l^*, l_0^* and ρ as defined above, equations (5) and (7) may be simplified as follows:

$$\frac{dn}{dt} = \left[(\phi\Sigma_f \{1 - \beta\}\nu + \sum_{i=1}^{6} \lambda_i C_i) p_{th}\right] - \phi(\Sigma_a + \Sigma_l) + S_0$$

$$\frac{dn}{dt} = \left[\frac{1}{l_0^*} n (1 - \beta) + p_{th} \sum_{i=1}^{6} \lambda_i C_i\right] - \frac{n}{l^*} + S_0$$

$$= \frac{n}{l_0^*}\left(1 - \beta - \frac{1}{K_{eff}}\right) + p_{th} \sum_{i=1}^{6} \lambda_i C_i + S_0$$

or $$\frac{dn}{dt} = \frac{\rho - \beta}{l_0^*} n + p_{th} \sum_{i=1}^{6} \lambda_i C_i + S_0 \qquad (13)$$

Likewise, from (5), $\lambda_i C_i = \left(\Sigma_f \phi \beta_i \nu - \frac{dC_i}{dt}\right)$

or $$\lambda_i C_i = \frac{\beta_i}{l_0^* p_{th}} n - \frac{dC_i}{dt} \qquad (14)$$

Equations (13) and (14) are the desired transient equations.

Finally, a single governing equation can be written by a simple substitution of (14) into (13) as follows:

$$\frac{dn}{dt} = \frac{\rho - \beta}{l_o^*} n + P_{th} \sum_{i=1}^{6} \left(\frac{\beta_i}{l_o^* P_{th}} n - \frac{dC_i}{dt} \right) + S_o$$

$$= \frac{\rho}{l_o^*} n - \frac{\beta}{l_o^*} n + \frac{\beta}{l_o^*} n - P_{th} \sum_{i=1}^{6} \frac{dC_i}{dt} + S_o$$

$$= \frac{\rho}{l_o^*} n - P_{th} \sum_{i=1}^{6} \frac{dC_i}{dt} + S_o$$

$$\text{or } l_o^* \frac{dn}{dt} = \rho n - l_o^* P_{th} \sum_{i=1}^{6} \frac{dC_i}{dt} + l_o^* S_o \qquad (15)$$

It will be further assumed that the so-called one-group theory is sufficiently accurate for accomplishing the goal at hand. In one group theory it is supposed that all production, diffusion, and absorption of neutrons occur at a single energy, namely, the thermal energy. Although this is a considerable approximation, the final simulator circuit is thereby simplified and results are still quite satisfactory. Since this theory implies that all fission neutrons have thermal energies, the resonance escape probability, p, and the non-leakage probability during the slowing down process, $e^{-B^2\tau}$, do not affect the multiplication factor and, hence, become unity in equations (13) thru (15). The two terms are carried through in the development of the electrical analog, but no attempt is made to employ them as variables in the final circuit.

4. The Electrical Analog.

Equation (15) is now in a convenient form for a computer solution. The network given in Figure 1 will be shown to describe this differential

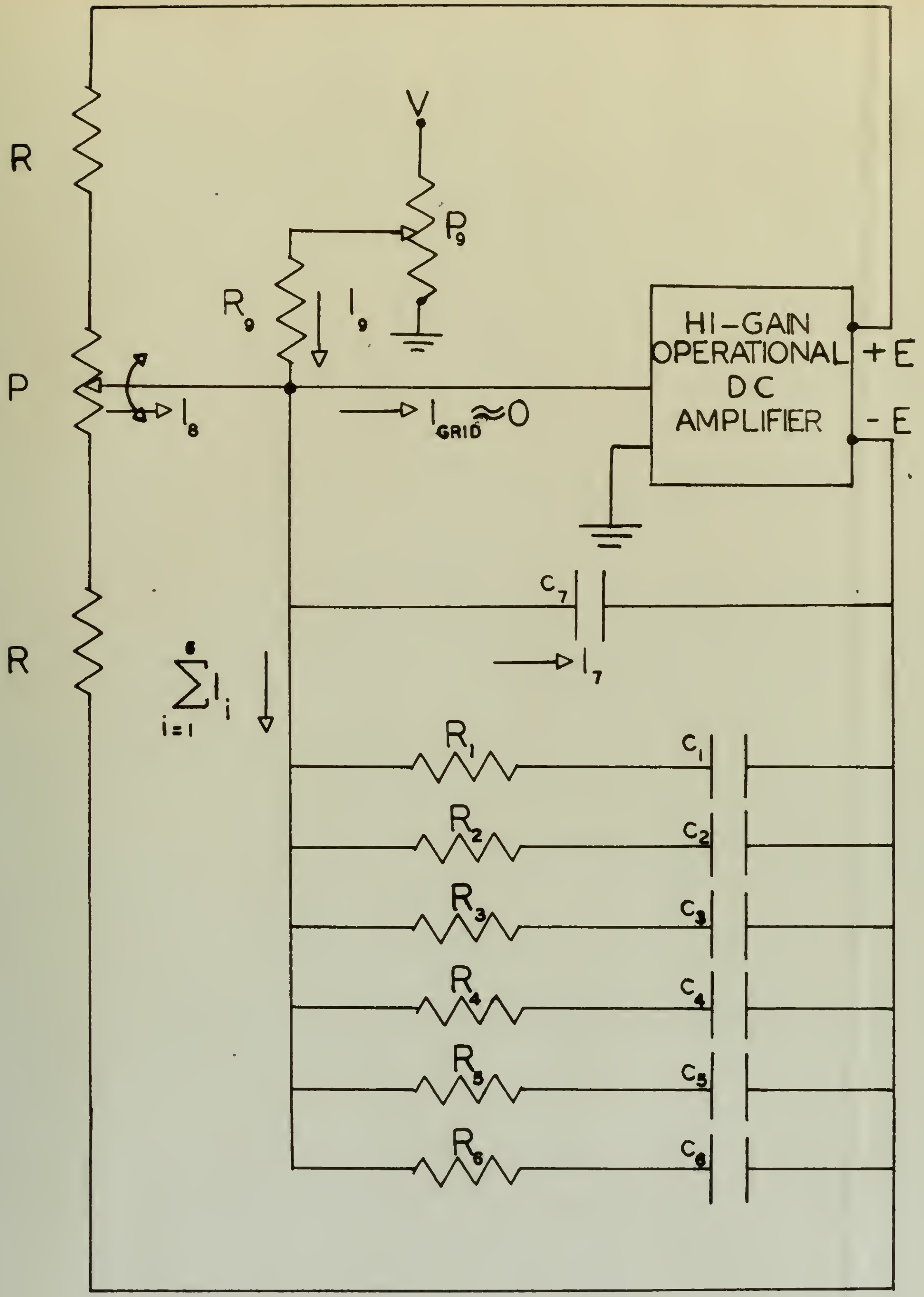

FIG. 1. BASIC REACTOR SIMULATOR CKT.

equation. Referring to Figure 1, and using Kirchoff's second law, it is evident that

$$I_7 = I_8 - \sum_{i=1}^{6} I_i + I_9$$

Note the similarity in form to (15).

The Rate Term $(l_o^* \frac{dn}{dt})$

$$I_7 = c_7 \frac{dE}{dt}$$

and letting E in volts be proportional to n in neutrons per cm³ per sec by the constant ζ, i.e., $E = \zeta n$, then

$$I_7 = \left\{ \frac{\zeta c_7}{l_o^*} \right\} l_o^* \frac{dn}{dt} \qquad (16)$$

The Reactivity Term (ρn)

Let Δ be the proportional distance of the potentiometer tap (at P) from the center of the potentiometer. Referring to the more detailed development given in Appendix I,

$$I_8 = \frac{\Delta E}{R \left[1 + R/P + P/4R \left(1 - \Delta^2 \right) \right]}$$

The range of values of Δ are zero at the center, + 1 at the + E end, and -1 at the -E end. Now, it is apparent that I_8 will have its maximum positive value at $\Delta = +1$. Therefore, the range of reactivity variation of the simulator may be set and the proper scaling factor determined by setting

$$\frac{\rho}{\rho_{max}} = \frac{I_8}{I_{8\ max}}$$

or $$\rho = \frac{\Delta}{1 + \frac{P^2}{4R(R + P)}(1 - \Delta^2)}\rho_{max} \qquad (17)$$

Since $I_{8\ max}$ occurs at $\Delta = 1$, then

$$I_{8\ max} = \frac{E}{R(1 + R/P)}$$

and therefore,

$$I_8 = \frac{E}{R(1 + R/P)} \frac{\rho}{\rho_{max}}$$

Again representing E by $\mathcal{J} n$, this reduces to

$$I_8 = \left\{\frac{\mathcal{J}}{R(1 + R/P)\rho_{max}}\right\}\rho\, n \qquad (18)$$

More careful consideration of (17) above reveals that ρ is a non-linear function of Δ which is undesirable for our purposes. This is due to the potentiometer loading having its greatest effect around the mid-position of the potentiometer. Linearity can be very closely approximated, however, by making R sufficiently large in relation to P that the denominator of (17) becomes essentially unity, leaving

$$\rho \approx \Delta\, \rho_{max}$$

If, for example, R=5P, the linearity remains below one percent for any value of Δ from (-)1 to (+)1.

The Delayed Precursor Term $\left(l_o^* \; p_{th} \sum_{i=1}^{6} \frac{dC_i}{dt}\right)$

The $\sum_{i=1}^{6}$ term of (15) is simulated by the six $R_i c_i$ delay networks. The basic voltage equation describing the voltage drop across any of the i^{th} type networks is

$$E = \frac{Q_i}{c_i} + R_i \frac{dQ_i}{dt}$$

where Q_i is the capacitor charge in coulombs and c_i is the capacitance of the i^{th} group. The electrical charge is analogous to the "storing" of delayed neutrons in the fission fragments before they are emitted. The corresponding delayed neutron equation represented by these networks is (14), which upon rearranging becomes

$$n = \frac{l_o^* \; p_{th} \; \lambda_i C_i}{\beta_i} + \frac{l_o^* \; p_{th}}{\beta_i} \frac{dC_i}{dt}$$

Again letting $E = \zeta n$ and matching terms with the basic equation above,

$$Q_i = \frac{\zeta \; l_o^* \; p_{th}}{\beta_i \; R_i} C_i \quad \text{and} \quad R_i \; c_i = \frac{1}{\lambda_i}$$

Now, $I_i = \frac{dQ_i}{dt} = \left(\frac{\zeta}{\beta_i R_i}\right) l_o^* \; p_{th} \frac{dC_i}{dt}$;

and by substitution for $\frac{dC_i}{dt}$ from (14),

$$I_i = \left(\frac{\mathcal{J}}{\beta_i R_i} \right) \beta_i \, n - \left(\frac{\mathcal{J}}{\beta_i R_i} \right) l_o^* \, p_{th} \, \lambda_i C_i$$

But, $\sum_{i=1}^{6} I_i = I_1 + I_2 + I_3 \ldots .$

and $\left\{ \frac{\mathcal{J}}{\beta_i R_i} \right\} l_o^* \, p_{th} \frac{dC_i}{dt} = \left\{ \frac{\mathcal{J}}{\beta_i R_i} \right\} \beta_i \, n - \left\{ \frac{\mathcal{J}}{\beta_i R_i} \right\} l_o^* p_{th} \sum_{i=1}^{6} \lambda_i C_i$ (19)

Therefore, $\beta_i R_i = \beta_1 R_1 = \beta_2 R_2 = \beta_3 R_3 \ldots \ldots$

The Source Term (S.)

If $R_9 \gg P_9$, then

$$I_9 \approx \frac{\Delta_9 \, V}{R_9}$$

where Δ_9 is the fraction off ground potential and V is a constant voltage source. Now, letting $\Delta_9 = \frac{S_o}{S_{o\,(max)}}$ then

$$I_9 = \left\{ \frac{V}{R_9 \, S_{o\,(max)} l_o^*} \right\} l_o^* \, S_o \qquad (20)$$

Finally, summing the currents as given by equations (16), (18), (19) and (20),

$$I_7 = I_8 - \sum_{i=1}^{6} I_i + I_9$$

$$\text{or } \left\{ \frac{\zeta c_7}{l_o^*} \right\} l_o^* \frac{dn}{dt} =$$

$$\left\{ \frac{\zeta}{R(1 + R/P)\rho_{max}} \right\} \rho n - \left\{ \frac{\zeta}{\beta_i R_i} \right\} l_o^* p_{th} \sum_{i=1}^{6} \frac{dC_i}{dt} +$$

$$\left\{ \frac{V}{R_9 S_{o\,(max)}\; l_o^*} \right\} l_o^* S_o \qquad (21)$$

In order for the current output of each term to be of the correct magnitude, the scaling factors which are enclosed by brackets in equation (21) must be identically equal to each other; that is,

$$\left\{ \frac{\zeta c_7}{l_o^*} \right\} = \left\{ \frac{\zeta}{R(1 + R/P)\rho_{max}} \right\} = \left\{ \frac{\zeta}{\beta_i R_i} \right\} = \left\{ \frac{V}{R_9 S_{o\,(max)}\; l_o^*} \right\} \qquad (22)$$

If this can be done, then these coefficients drop out of equation (21) leaving equation (15) which is to be duplicated electrically. Values to insert into (22) will be determined by constants in the actual system to be simulated as well as arbitrary values selected in accordance with standard computer operating techniques.

5. Simulation of a Specific Low Power Thermal Reactor —AGN-201

General thermal reactor simulation, therefore, can be readily duplicated by the circuit given in Figure 1. This circuit when set up on a conventional analog computer, using completely arbitrary circuit parameters, will yield typical time-flux curves. The problem at hand, however, is to simulate a specific reactor wherein lie many additional considerations which first must be resolved before a final circuit can be drawn up. These include detailed investigations to.

(1) determine actual range of reactivity variation, compute rates of reactivity change for control rod movement, and provide suitable means for duplicating control rod action;

(2) determine a means of introducing a maximum reactivity control and temperature coefficient of reactivity;

(3) solve electrical problems resulting from real time simulation over wide operating ranges of neutron flux from source level to full power;

(4) and to determine an appropriate value of neutron source voltage corresponding to the extraneous source production rate.

In the analysis of these problems, attention shall be restricted to the simulation of the low power thermal reactor currently installed at the United States Naval Postgraduate School. This reactor will hereinafter be referred to as the AGN-201.

Before solving the problems, it is necessary to mention a few essential features of the AGN-201 which will form the basis on which ultimate simulator construction may proceed. The general characteristics of the 201 reactor are listed in Table 1 below.

TABLE 1. GENERAL CHARACTERISTICS AGN-201

Power (licensed)	100 miliwatts
Maximum Thermal Flux @ 100 mw	$4.5 \times 10^{6} cm^{-2} sec^{-1}$
Critical Mass	665 gm U^{235}
Core Size (cylinder)	10" dia. x 9½" high
Moderator (polyethylene)	11 kgm
Reflector (graphite)	20 cm thick (1.70 gm/cm^3)
Shield (lead)	10 cm thick
(water)	55 cm thick (1000 gallons)
Over-all diameter	6½ ft
Over-all height	9 ft
Temperature coefficient of reactivity (based on water shield temp. data)	-2.75×10^{-4} /°C

Figure 2 shows the AGN-201 core tank containing the uranium-polyethylene core and portions of the graphite reflector. Figure 3 is a cross-sectional view of the entire reactor unit showing the core, reflector, lead and water shields, glory hole, and control rod assemblies. The critical mass consists of about 665 grams of U^{235} in the form of 20%- enriched UO_2. It is contained in the form of a powder dispersed in a solid polyethylene moderator. The core is made in nine sections of various thicknesses (Figure 2). Each of the four bottom discs has three 5-cm holes and one 2.5-cm hole. The 201 has two safety rods and two control rods. The three larger holes are for two safety rods and one coarse control rod while the smaller hole is for a fine control rod. The two safety rods and the coarse control rod are identical and each contain about 14 grams of U^{235}. The fine rod containsabout 3.5 grams of U^{235}. All rods operate so that reactivity is increased as the rod is inserted. The amount of reactivity each rod controls increases as the amount of active material contained increases. With the above amounts of U^{235} in the rods, the safety and coarse control rods control about 1.1% reactivity while the fine control rod controls about 0.3% reactivity. The rods are inserted by a reversible d-c motor drive mechanism requiring about one minute to travel the full 25-cm stroke. Referring to Table 1, the thermal flux at licensed full power is given as 4.5×10^6 neutrons /cm²/sec. This is well below that at which Xenon poisoning becomes a consideration, namely, at a flux in excess of about 10^{12} neutrons /cm²/sec. Finally, because of the low power developed, heating of the core is so slight that it is essentially ambient temperature which determines core temperature and, hence, the maximum reactivity available. The negative temperature coefficient listed in Table 1, therefore, is based on the change in temperature of the 1000

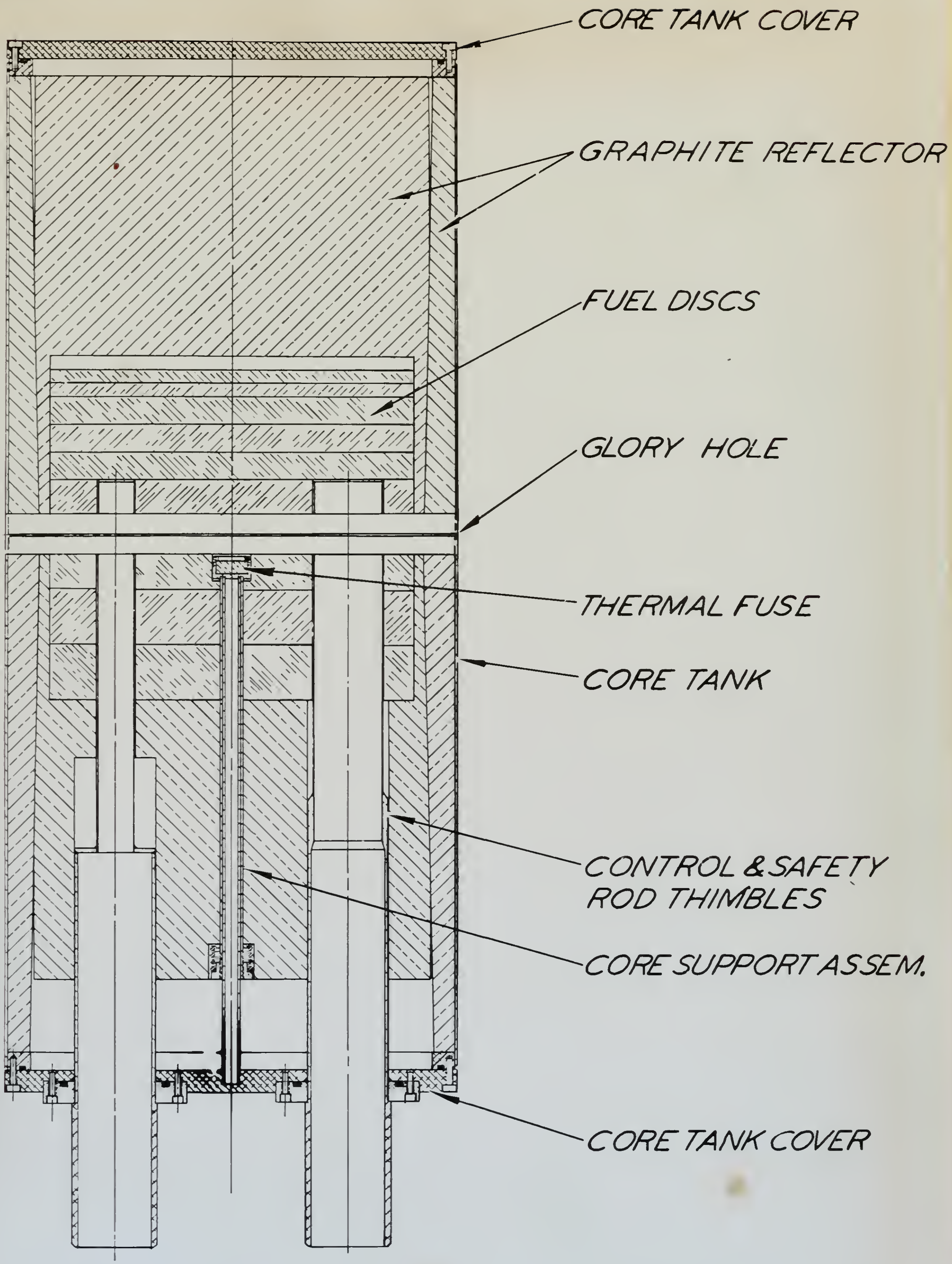

FIG. 2. VIEW OF SIMULATED REACTOR, AGN-201, CORE TANK ASSEMBLY

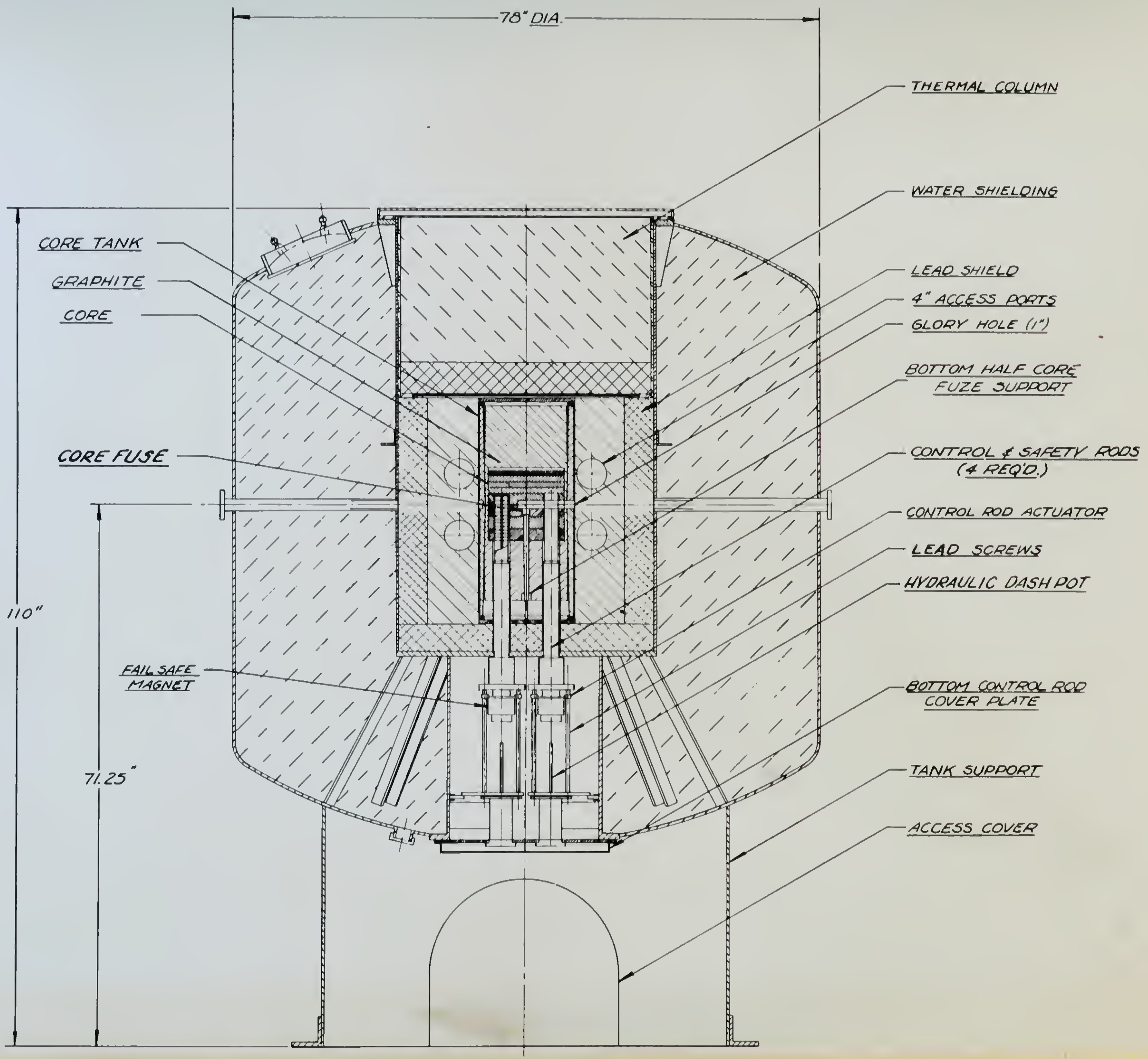

FIG. 3. CROSS-SECTIONAL VIEW AGN-201 SHOWING IMPORTANT FEATURES

gallon water shield surrounding the core tank {10}. With these features in mind, let us proceed with the investigations into the special problems mentioned.

First, a control rod calibration must be made, the result of which is shown graphically in Figure 4. The term relative reactivity as used here implies an arbitrary zero reactivity reference when the rods are fully retracted. As will be seen later, the major portion of the reactivity contribution or "worth" of the rods is employed in reducing the amount by which the reactor is subcritical. Only a small fraction of this relative reactivity is actually positive reactivity as defined by (8). This curve represents a superposition of data taken on both fine and coarse control rods which actually exist on the reactor, thus providing a single curve to represent the movement of both rods simultaneously. In view of the fact that the action of the two control rods on the reactor can be duplicated more simply and more economically on the simulator by a single controlling device, simulation of operation of each rod individually does not seem warranted. Now, under normal conditions, the reactor will be operating in the straight line portion of the curve when near-critical conditions exist. As indicated in Figure 4, the slope of this straight line is 837 $\mu\rho$ ($\rho \times 10^{-6}$) per cm of rod travel. From weight data on the fuel discs which make up the two safety rods and the fine and coarse control rods, it is found that the relative reactivity contribution of each safety rod is essentially equal to that of the coarse control rod or about 11,275 $\mu\rho$ each. Therefore, the total contribution in terms of relative reactivity of all rods is found to be 36,725 $\mu\rho$. The reactivity potentiometer can now be designed to match the control and safety rod curves. Figure 5 shows a plot of percent of total resistance

See bel

[illegible]

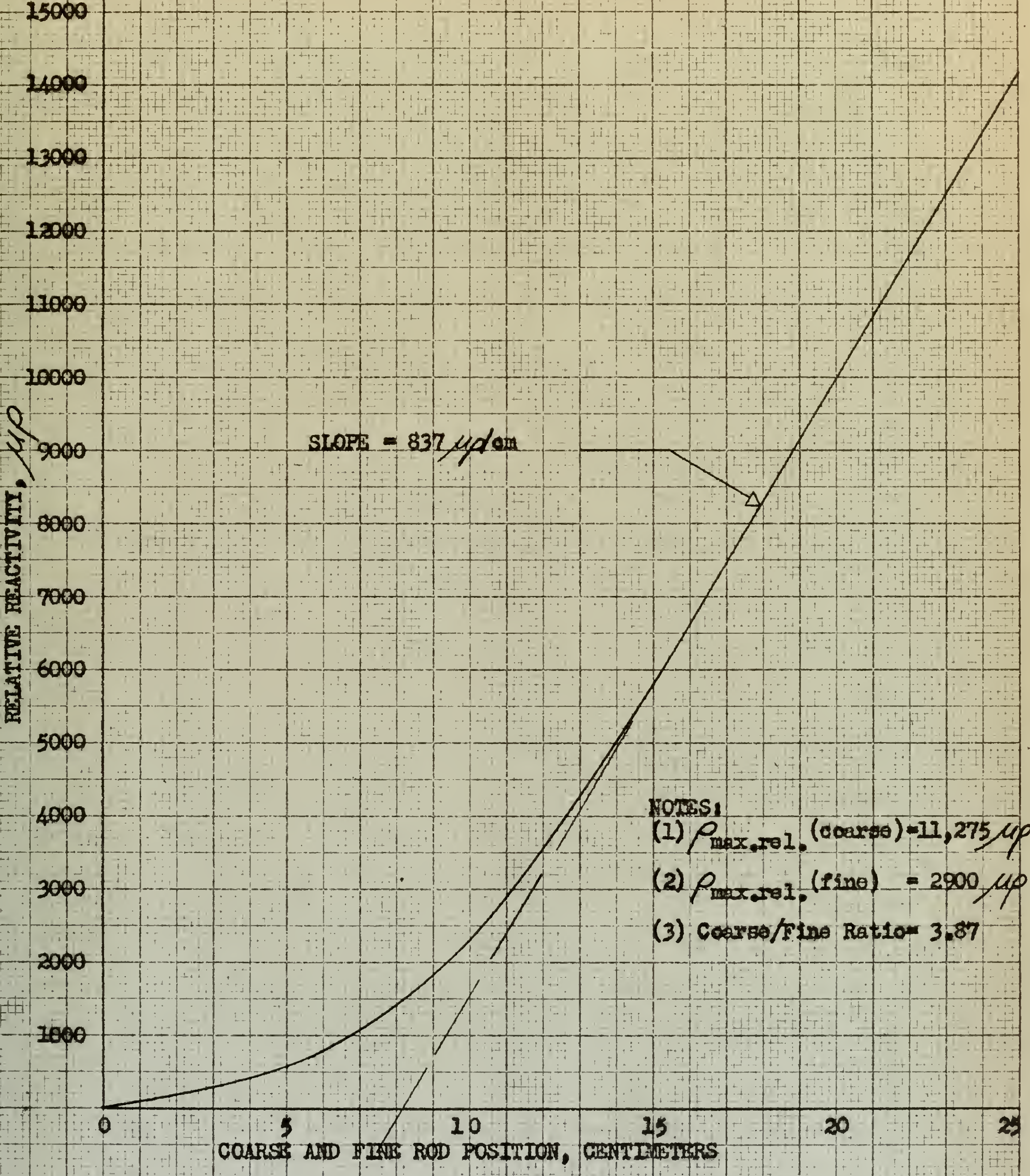

NOTES:

(1) $\rho_{\text{max.rel.}}$(coarse) = 11,275 $\mu\rho$

(2) $\rho_{\text{max.rel.}}$(fine) = 2900 $\mu\rho$

(3) Coarse/Fine Ratio = 3.87

FIG. 4. AGN-201 COMBINED COARSE AND FINE ROD CALIBRATION CURVE

of the reactivity potentiometer versus percent of total rotation (about 350°) where all rods are being considered. Notice that the curve is shown up to the point at which the safety rods are completely inserted as a dashed line. Because the safety rods are not utilized for control purposes, their individual calibration curves are of no concern as long as their ultimate contribution to total relative reactivity is known, namely, 22,550 $\mu\rho$ or about 61.4% of the total available for addition by rod insertion. From this point on, however, it would be desirable to follow the remainder of the curve which is essentially Figure 4 superimposed but plotted using non-dimensional relationships. To duplicate the entire curve precisely would require a non-linear potentiometer which could be designed but at considerable expense. Instead, in view of the fact that the straight line portion of the combined control and calibration curve is of greatest interest, a center-tap potentiometer permits precise duplication in this region. At 50% rotation, extrapolation of the straight line portion back to this point reveals that 25% total resistance should result at this point. For the 20,000 ohm potentiometer selected, this requires a 5000 ohm resistor in parallel with the first half of the potentiometer. The arrangement is shown schematically in Figure 5; and the actual plot of percent resistance versus percent rotation resulting is indicated by circles in the figure. It is noted that 61.4% of the total resistance will now occur at about 75% of total potentiometer rotation. If this point is denoted for the simulator as having a control rod position reading of zero, then a discrepancy will exist between the control rod-reactivity relationships of the actual reactor and that of the simulator. As seen from Figure 5, the simulator rods increase reactivity linearly over their entire travel while actual rod insertion increases reactivity linearly only over the last 10 cm of travel. This situation must be accepted when

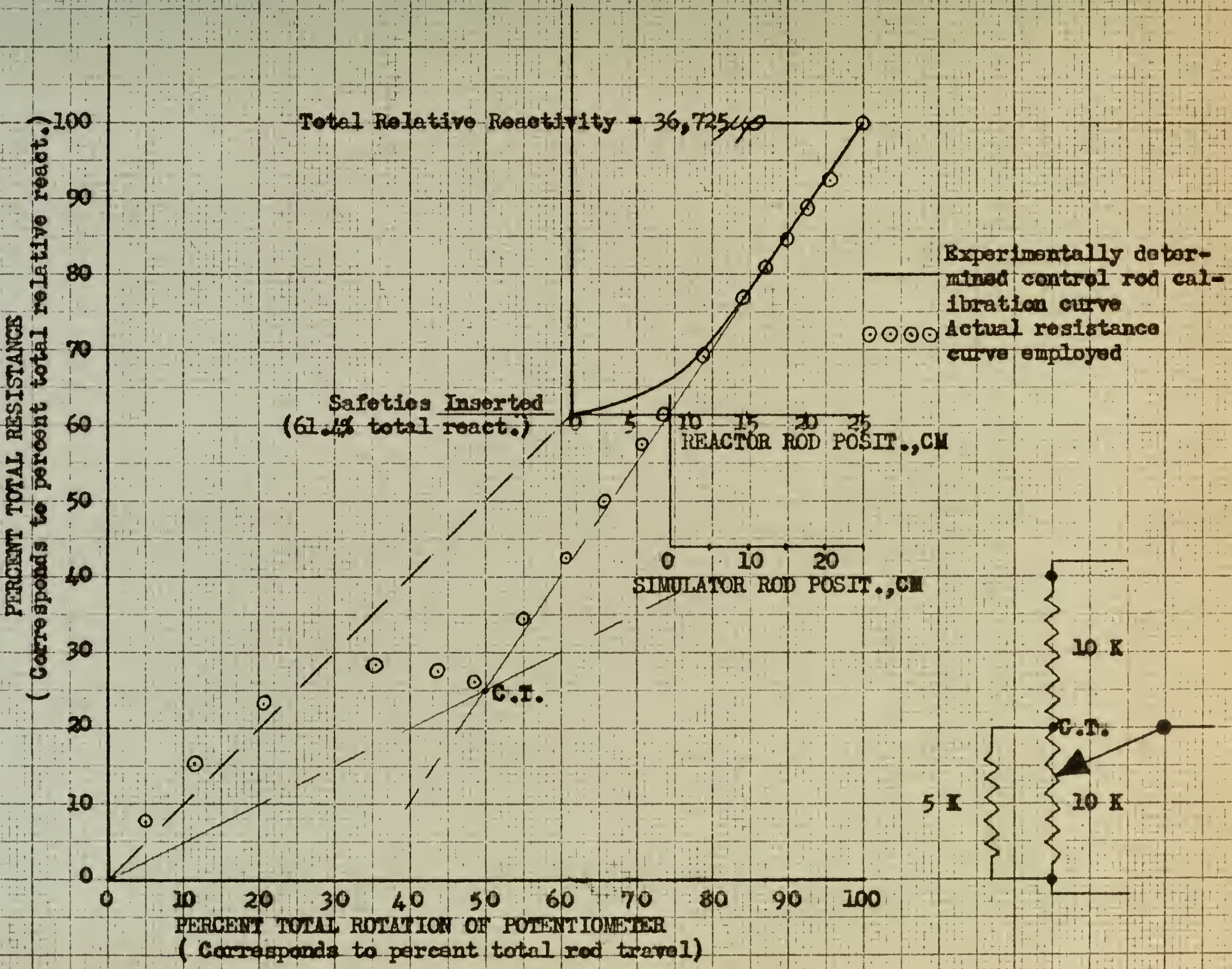

FIG. 5. REACTIVITY POTENTIOMETER CALIBRATION CURVE

the actual reactivity curve cannot be duplicated over its entire range. The rate of potentiometer rotation is easily obtainable by timing the actual control rod insertion rate. Both fine and coarse control rods have been set to move from the fully retracted to the fully inserted positions (0 to 25 cm.) in about one minute at the fast speed setting. Therefore, the last 10 cm of actual rod travel will be completed in 0.40 min. From Figure 5 the last 10 cm of actual rod travel commences at 85% of total potentiometer rotation or, alternately, over the last 0.15 revolution. Hence, the reactivity potentiometer drive rate should be 0.15 revs/0.40 min = .37 rpm. at the proper rate. Over this straight line portion, reactivity change at fast speed is found to be

$$837 \ \mu\rho \ /\text{cm} \times \frac{25}{60} \ \text{cm/sec} = 349 \ \mu\rho \ /\text{sec}$$

To solve the second problem, a means of establishing a variable zero or critical reference level must be provided for the reactivity potentiometer. The reactor functions between certain definite reactivity limits for any specified core temperature. In other words, some scheme is required to duplicate the normal operating ranges to be expected from maximum subcritical conditions to maximum supercritical conditions. For example, at 23°C, the maximum positive reactivity attained with all rods fully inserted is only about .0020. At the same time, with all rods fully retracted, the reactor has a negative reactivity of about .035. This one-sided variation is representative of the type of reactivity behavior encountered under typical operating conditions. It should be noted here that the above values were determined with the so-called "glory hole" empty. The glory hole (Figure 2) is a small access tube about one inch in diameter

[illegible] a motor [illegible] friction clutch [illegible] made.

which passes through the core center, and into which additional fuel, moderator, reflector material, samples and the like can be inserted to yield changes in reactivity. As an example, by insertion of the proper amounts of moderator, reflector, and lead shielding in the glory-hole, the core is made essentially homogeneous; and an additional reactivity contribution of about 2600 $\mu\rho$ can be realized. Moreover, an average linear temperature coefficient of reactivity, based on water shield temperature, of about -2.75×10^{-4} per °C exists for the AGN-201. This rather significant effect on reactivity must also be taken into consideration. Figure 6 represents the scheme devised to yield the proper operating range of reactivity from a relatively large negative value to a small positive value and, in addition, to permit control over maximum positive reactivity available. A permanently imposed offbalance in the values of R_1 and R_2 will electrically offset the mechanical mid-position as indicated. The values given in the figure are those based on the reactivity conditions at 23°C and employing a homogeneous core. The critical or zero position is now located at point C. In addition, it is noted that C can be further controlled by movement of the maximum reactivity control and temperature coefficient (MRCTC) potentiometer. If, for example, the temperature increases (or alternately, if a sample with a large thermal neutron absorption cross-section is placed in the glory hole), the MRCTC potentiometer is moved as indicated in the figure. This increases the resistance in loop 2 and decreases the resistance in loop 1, causing an unbalance in the feedback circuits, thereby producing a decrease in reactivity corresponding to the amount of resistance change applied. If, therefore, it is desired to hold the reactivity at zero, the reactivity potentiometer must be moved in such a direction as to balance the resistances in the two loops. In this case,

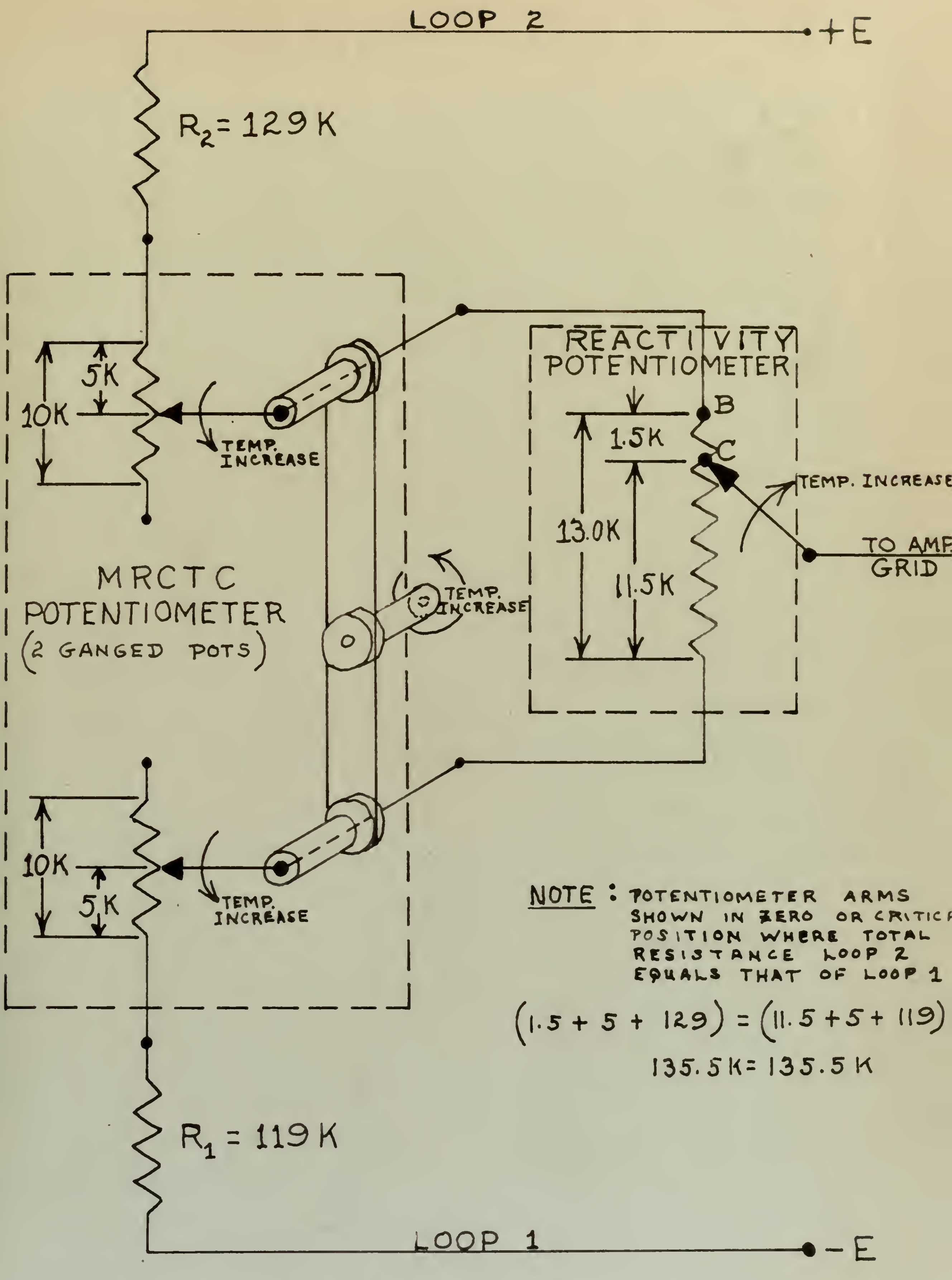

NOTE: POTENTIOMETER ARMS SHOWN IN ZERO OR CRITIC POSITION WHERE TOTAL RESISTANCE LOOP 2 EQUALS THAT OF LOOP 1

$$(1.5 + 5 + 129) = (11.5 + 5 + 119)$$

$$135.5\text{K} = 135.5\text{K}$$

FIG. 6. MAX. REACT. CONTROL & TEMP. COEFFICIENT POTENTIOMETER SCHEMATIC

it would require movement of the arms as indicated. It can readily be seen that if the temperature coefficient is offset far enough, the maximum positive reactivity available can be reduced until the reactor may no longer be brought critical even though all rods are inserted. This corresponds to the point marked B in the figure. The original electrical center position C, therefore, effectively walks up and down the reactivity potentiometer depending on the setting of the MRCTC potentiometer. Of course, maximum positive reactivity may likewise be increased to prompt critical conditions and above if desired. One of the solutions of the transient equations for a step change in reactivity is the so-called Inhour equation. The plot of this equation using the value of neutron lifetime applicable to the AGN-201 is given in Figure 7. Calibration of the MRCTC potentiometer can be made by measuring the stable period (T) for any particular potentiometer setting when all rods are fully inserted. The corresponding reactivity may then be picked off an appropriate plot of the Inhour equation using the neutron lifetime applicable to the reactor being simulated. Such a calibration curve is given in Figure 8 for the particular MRCTC potentiometer employed here. Temperatures shown in the figure are based on experimental data employing a homogeneous core and using the negative temperature coefficient of reactivity from Table 1. In summary, therefore, the MRCTC potentiometer functions as an electrical stop on the upper limit of the reactivity potentiometer which provides a scheme to preset any desired maximum reactivity (or alternately, any desired core temperature). The effect on the electrical circuit can be taken into account quite simply as is indicated in Appendix II.

[illegible]

The third problem can be solved by employing stablized operational amplifiers with virtually zero drift to give reasonably accurate and reproducible solutions at the extremely low starting or source voltages encountered.

George A. Philbrick Researches, Inc. Boston 16, Mass.
K2-X amplifiers; K2-P stabilizers; R-100, power supply.
cost for 3 ampl., 3 stab., and 1 power supply $367

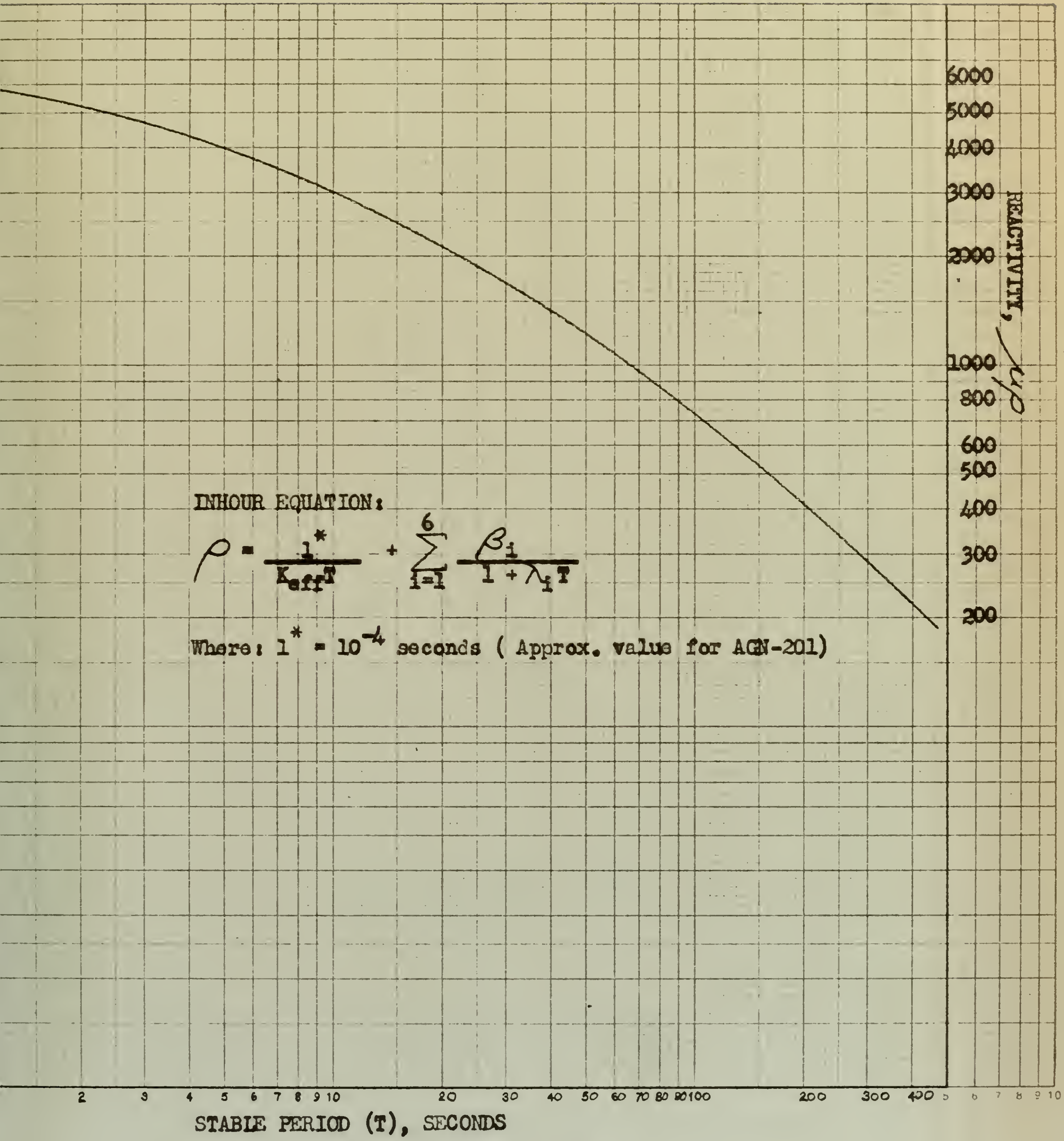

INHOUR EQUATION:

$$\rho = \frac{l^*}{K_{eff}T} + \sum_{i=1}^{6} \frac{\beta_i}{1 + \lambda_i T}$$

Where: $l^* = 10^{-4}$ seconds (Approx. value for AGN-201)

FIG. 7. PLOT OF THE INHOUR EQUATION

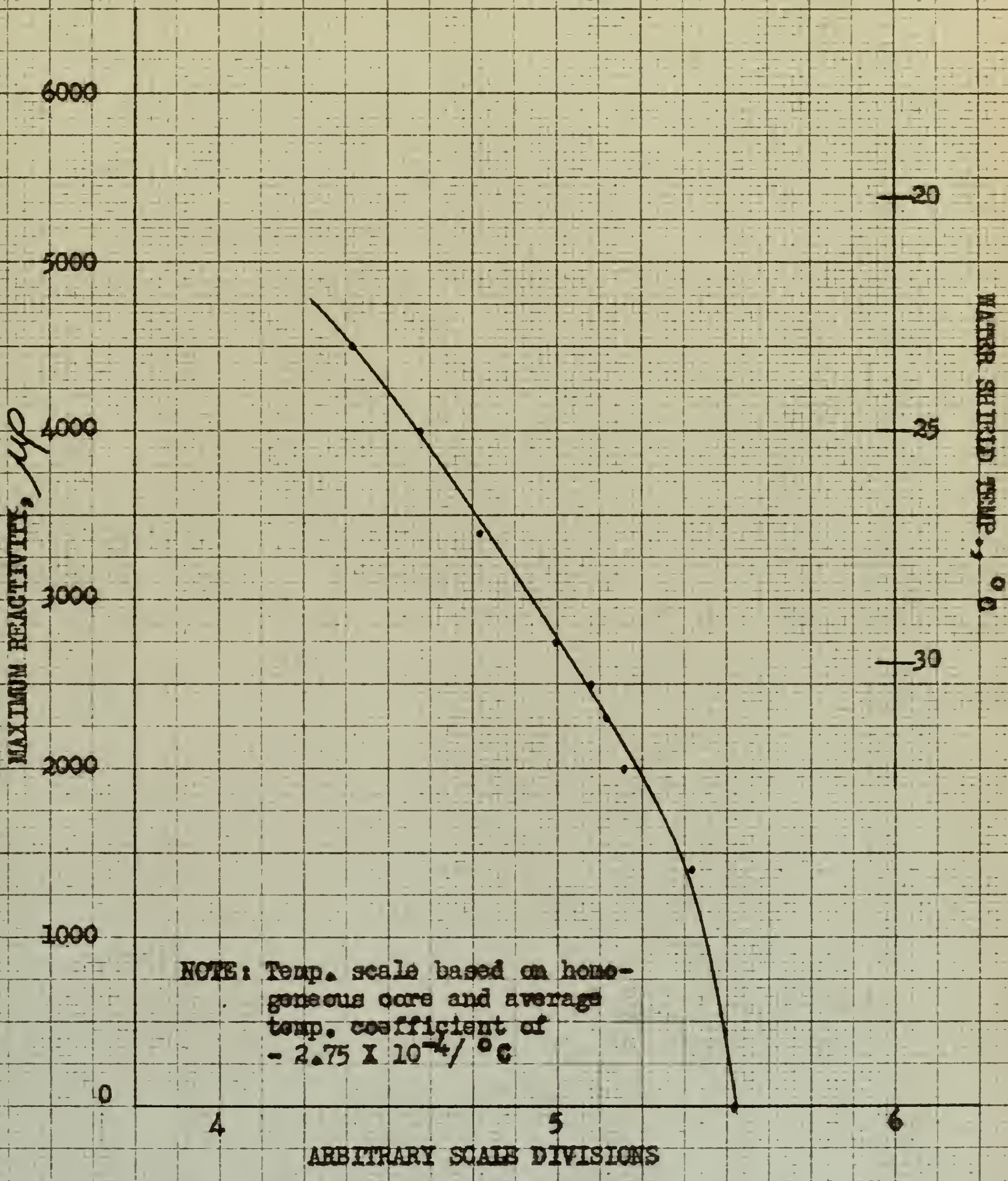

FIG. 8. MRCTC POTENTIOMETER CALIBRATION CURVE

The latter are of the order of magnitude of a few millivolts if scaling is such as to have about four decades of multiplication from source level to full power. The maximum output of the amplifiers is 100 volts. A variable biasing arrangement is also desirable to ensure zero offset at zero voltage input to the amplifier gird. Any one of several suitable methods recommended by the manufacturer of the amplifiers will satisfy this requirement. Causing additional problems at low operating voltages are the condensers in the circuit. It is found that an erroneous flux-time curve results in the low voltage region upon the decay of the neutron flux when the reactor simulator is scrammed. Analysis of oil, paper, mica, electrolytic, and other types of commonly used capacitors reveals a marked dielectric absorption effect by which these types hold their charge for a relatively long period of time even after direct shorting across the terminals. This problem is virtually eliminated by the use of polystyrene or mylar condensers which exhibit characteristically low dielectric absorption properties.

The fourth and final problem is significant only in that it is considered desirable to simulate reactor responses over the entire operating range. This demands computer solutions to the controlling equations at extremely low values of neutron flux which corresponds to the condition in the reactor when all rods are retracted, and the existing neutron density is dependent on the extraneous neutron source strength. This problem may be approached as follows: From equation (15), namely,

$$l_o^* \frac{dn}{dt} = \rho n - l_o^* P_{th} \sum_{i=1}^{6} \frac{dC_i}{dt} + l_o^* S_o$$

it is apparent that under steady-state conditions $\frac{dn}{dt}$ and $\frac{dC_i}{dt}$ terms drop out leaving

$$\rho n + l_0^* S_0 = 0$$

or rearranging,

$$S_0 = \frac{-\rho n}{l_0^*} \tag{23}$$

And from equation (8) and (9), this can be written as

$$S_0 = \frac{n(1 - K_{eff})}{l^*} \tag{24}$$

From manufacturer's data or from actual experimental flux determinations, a value of n can be calculated at a level where reactivity is known. The latter is obtainable from experimentally determined control rod calibration data. Employing (23), this will establish a value of $S_0 l_0^*$ at one particular control rod position. From the known value of reactivity at this position, K_{eff} may be determined from (8). Finally, from (24), $S_0 l^*$ is obtained. If the value of estimated neutron lifetime as given by the manufacturer is then employed, S_0 is readily calculated. It is noted from (22) that

$$\frac{V}{R_9 S_{0\,(max)}\, l_0^*} = \frac{\zeta}{R(1 + R/P)\rho_{max}}$$

or rearranging,

$$V = \frac{\zeta\, R_9\, (S_{0\,(max)}\, l_0^*)}{R(1 + R/P)\,\rho_{max}}$$

Therefore, to obtain the neutron source voltage corresponding to a particular source generation rate, the product $(S_{0\,(max)}\, l_0^*)$ need only be determined

as accomplished above, and actually the two terms need not be separated to determine the voltage. The magnitude of neutron lifetime itself is important in the determination of a proper value of the integrating capacitor c_7. From (22)

$$c_7 = \frac{l_o^*}{R(1 + R/P)\,\rho_{max}}$$

or, essentially, c_7 is proportional to neutron lifetime. However, if the order of magnitude of neutron lifetime is known, this is sufficiently accurate to yield excellent results as long as maximum reactivity values are limited to .005 and under. This figure of .005 is arrived at by evaluating the stable period corresponding to various values of positive reactivity when different neutron lifetimes are considered. The Inhour Equation may be employed to make this comparison analytically; and it will be found that, at low reactivities, period is independent of neutron lifetime for a specified reactivity. Furthermore, in view of the fact that the stable period corresponding to a neutron lifetime of 10^{-4} sec and a reactivity of .005 is about 2.5 seconds, this condition on the actual reactor cannot be duplicated because a period scram is set to function at about 3.0 seconds. As a consequence, comparison runs at higher values of reactivity to better evaluate neutron lifetime are not feasible.

Having solved the above four problems, the remaining circuit parameters may be calculated as indicated in Appendix II and the final AGN-201 simulator can be constructed. Figure 9 is a schematic of the final analog, and listed in Table 2 below are the various values of circuit components referred to in the figure. Also listed are the other factors which appear in the scaling factor equation (22).

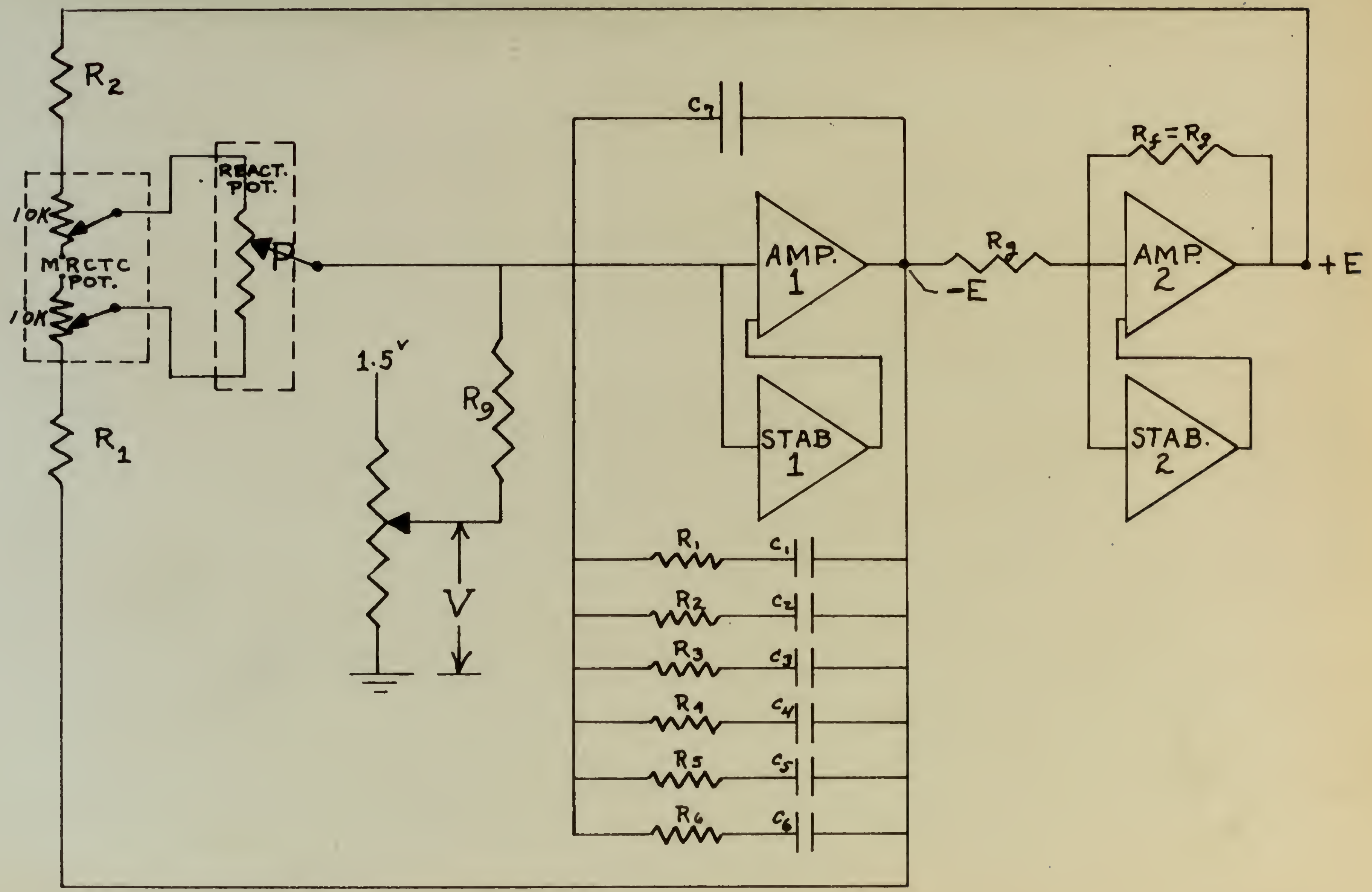

FIG. 9. AGN-201 ELECTRICAL ANALOG SCHEMATIC

TABLE 2a. CIRCUIT VALUES

P = 13.0 KΩ (actual value of pot.)

R_1 = 119 KΩ

R_2 = 129 KΩ

c_1 = .0007 μf R_1 = 102M

c_2 = .0207 μf R_2 = 30M

c_3 = .208 μf R_3 = 10.6M

c_4 = .544 μf R_4 = 12.0M

c_5 = 2.06 μf R_5 = 15.4M

c_6 = .785 μf R_6 = 102M

c_7 = .0039 μf

R_g = R_f = 1M

R_9 = 10M

V = 51mv

TABLE 2b. ADDITIONAL SCALING FACTOR VALUES

P_{eff} = 23.0KΩ (use for P in equation 22)

R = 119KΩ (use for R in equation 22)

ρ_{max} = .034775 @ 23°C (core homogeneous)

β_1 = .00025

β_2 = .00085

β_3 = .00241

β_4 = .00213

β_5 = .00166

β_6 = .00025

$\mathcal{J}$ = 2.22

S_0 = $S_{0\,(max)}$ = .579 neuts/cm^3/sec

$l^* \approx 1.0 \times 10^{-4}$ sec $\approx l_0^*$ near critical

$$(\text{i.e. } K_{eff} \approx 1)$$

Figure 10 is a photograph of the completed simulator with linear recorder unit attached. Important features and actual circuitry are shown in Figure 11 which is a rear view of the simulator console. At the left center of Figure 11 is the reactivity potentiometer and drive motor assembly; at the upper right portion of the figure is the MRCTC potentiometer; and at the bottom portion of the photograph is the entire simulator circuit which is constructed to resemble the schematic of Figure 9. Along the top of the console are located the operational amplifiers and stabiliting amplifiers.

6. Degree of Simulation Attained

Figures 12 through 14 represent comparison flux-time plots taken from the reactor and the simulator, utilizing the same linear recorder so as to ensure an identical time base. The sequence of events describing each of the comparison runs is briefly discussed in the succeeding paragraphs.

The sequence of events describing Figure 12 is given in Table 3.

TABLE 3. SEQUENCE OF EVENTS FOR FIGURE 12

TIME IN MINUTES	REACTOR SEQUENCE	CORRESPONDING SIMULATOR SEQUENCE
—	Steady flux level; rods @ 15 cm; glory hole empty; temp. 21°C.	Steady flux level; rods @ 10.1 cm; MRCTC set for proper max. reactivity conditions.
0	Inserted rods @ fast speed.	Inserted rods @ fast speed.

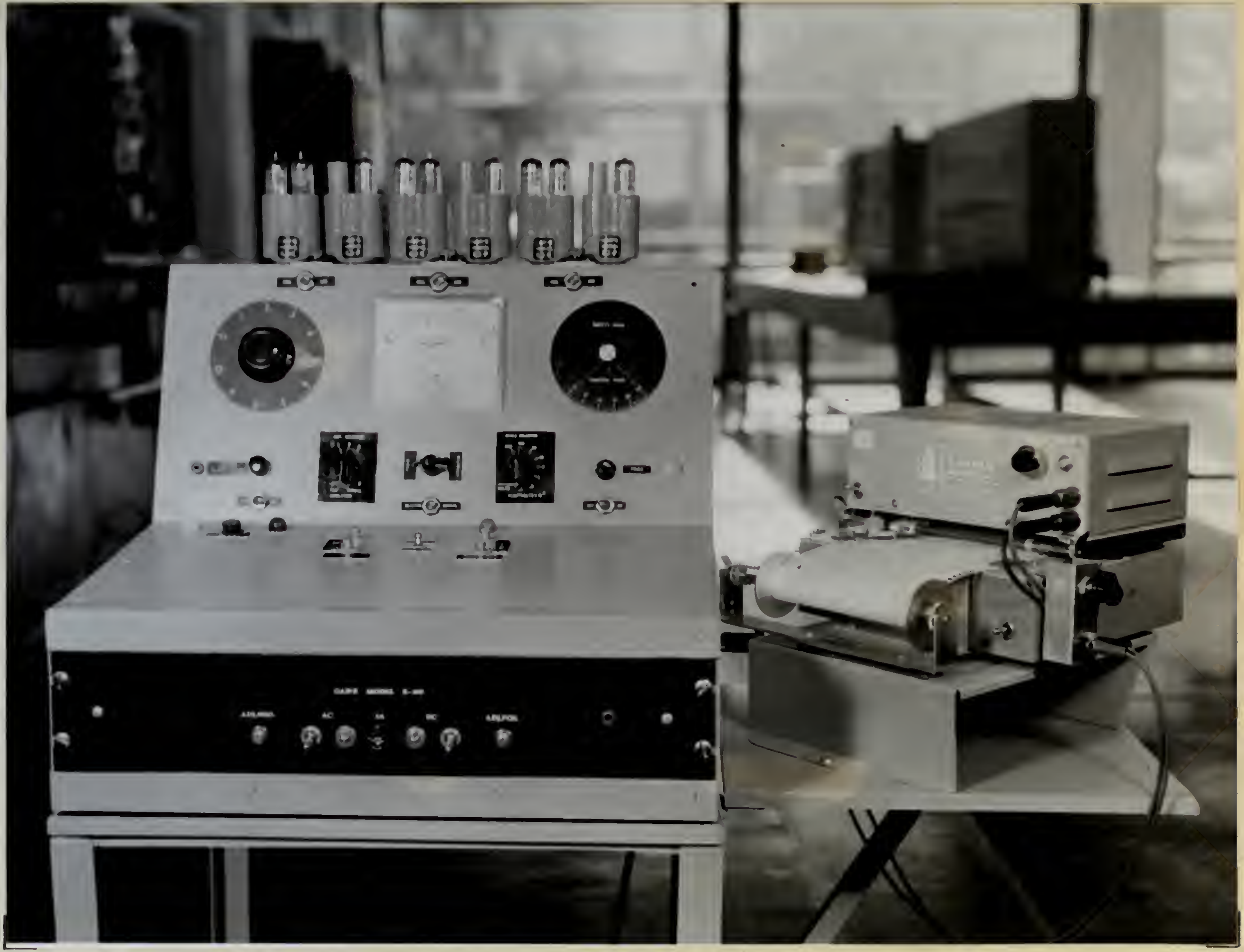

FIG. 10. VIEW OF COMPLETED SIMULATOR WITH LINEAR RECORDER ATTACHED

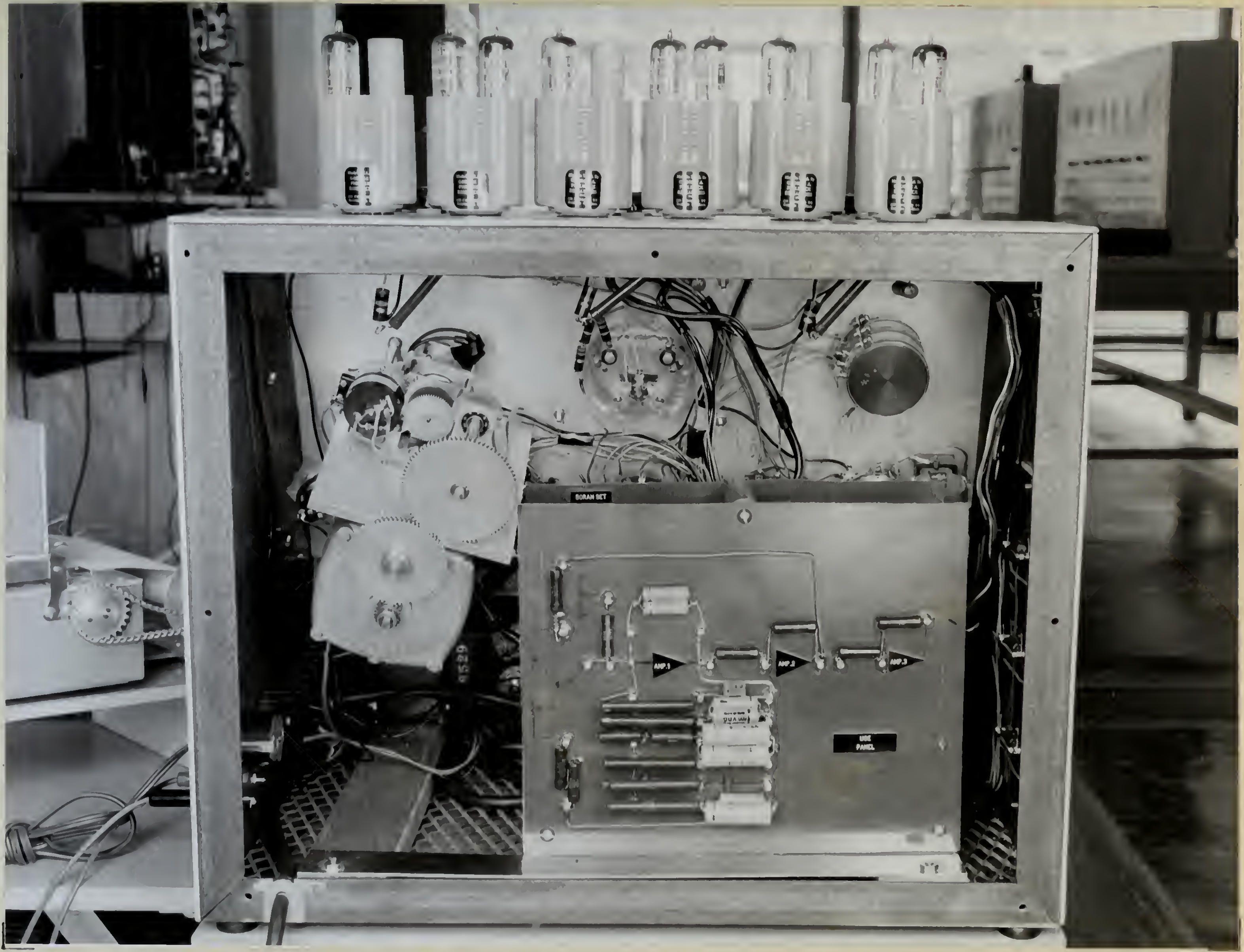

FIG. 11. REAR VIEW OF SIMULATOR CONSOLE

0.4	Rods up; flux permitted to increase on 17.5 sec. period	Rods up; flux permitted to increase on 17.5 sec. period.
2.1	Flux level 7.6 x 10^6 (0.76 x 10^{-8} μμa scale reading); rods retracted to 20.45 cm; flux permitted to decay to 1.0 x 10^6.	Flux level @ 7.6 x 10^6 (76 volts scale reading) rods retracted to 22.5 cm; flux permitted to decay to 1.0 x 10^6.
4.25	Adjusted rods for steady flux level.	Adjusted rods for steady flux level.
7.50	Quickly inserted moderator, graphite, and lead discs into glory hole to provide a step change of about (+) 1300 $\mu\rho$ ($\frac{1}{2}$ of total required to make core essentially homogeneous.)	Quickly rotated MRCTC potentiometer to provide corresponding (+) 1300 $\mu\rho$ step change in reactivity.
8.65	Retracted rods to 19.93 cm; allowed flux to decay to 4.0 x 10^6.	Retracted rods to 21.9 cm; allowed flux to decay to about 4.0 x 10^6.
10.15	Inserted remainder of poly, graphite, and lead in glory hole and adjusted rods to steady flux level of 4.5 x 10^6 - rated power 100 mw.	Rotated MRCTC potentiometer an additional amount corresponding to about 1300 $\mu\rho$ to simulate homogeneous core conditions and brought to steady flux level of 4.5 x 10^6.
12.05	Quickly withdrew all poly from glory hole to provide a step change of about (-) 2600 $\mu\rho$; allowed flux level to decay to about 0.63 x 10^6.	Quickly reset MRCTC to original setting corresponding to glory hole empty conditions thus providing a step change in reactivity of about (-) 2600 $\mu\rho$; allowed flux to decay to about 0.54 x 10^6.
13.5	Inserted rods all the way; permitted flux to increase to about 4.5 x 10^6 and leveled at about 4.0 x 10^6.	Inserted rods all the way; permitted flux to increase to about 4.5 x 10^6 and leveled at about 4.0 x 10^6.

As indicated in Table 3, the position to which simulator rods are retracted in each case is different from that given by the rod position indicator on

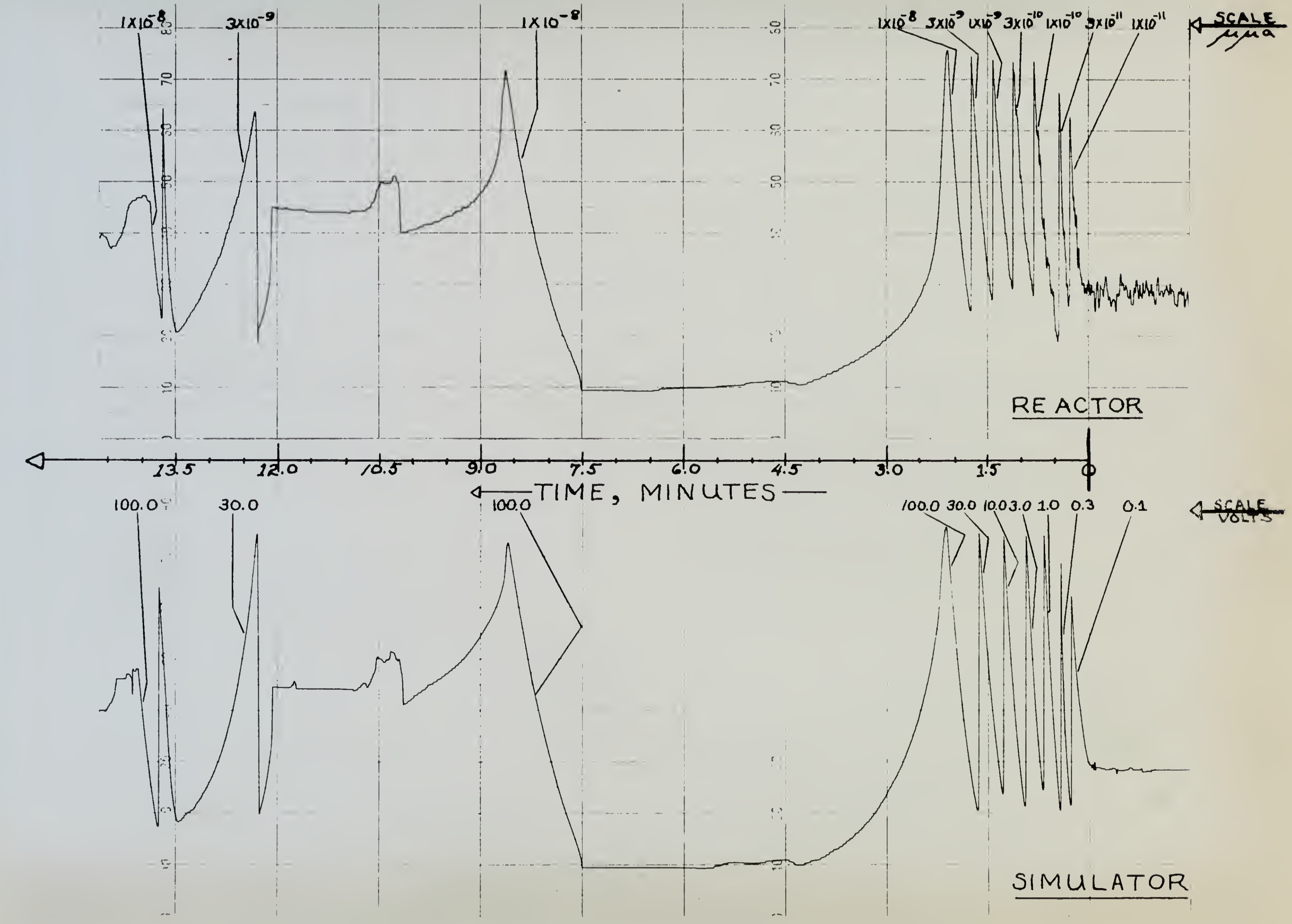

FIG. 12. FLUX-TIME COMPARISON CURVES

the reactor console. This implies that the reactivity potentiometer contributes more reactivity per centimeter of movement than do the actual rods. By a trial and error procedure of slightly altering the value of the paralleling resistance of the reactivity potentiometer, the actual and simulator rod positions might be more closely brought into agreement.

The sequence of events describing Figure 13 is given in Table 4.

TABLE 4. SEQUENCE OF EVENTS FOR FIGURE 13

TIME IN MINUTES	REACTOR SEQUENCE	CORRESPONDING SIMULATOR SEQUENCE
—	Approximately steady flux level; rods @ 15 cm; glory hole empty; temp. 21°C.	Steady flux level; rods @ 10.1 cm; MRCTC potentiometer set for proper maximum reactivity conditions.
0	Inserted rods at fast speed.	Inserted rods at fast speed.
0.4	Rods up; flux permitted to increase on 17.5 sec. period.	Rods up; flux permitted to increase on 17.5 sec. period.
2.1	Retracted rods and brought to steady flux level of 7.0×10^6.	Retracted rods and brought to steady flux level of 7.0×10^6.
3.0	Scrammed reactor and permitted flux to decay to observe effects of delayed neutrons.	Scrammed simulator and permitted flux to decay to observe effects of delayed neutron networks.

Simulation on scramming the reactor is difficult to reproduce because of dashpot action on the rods as they are ejected from the core. This action was approximated by manually rotating the reactivity potentiometer to the all-rods-out position. As a result, the simulator decay curve on scramming appears to be steeper than the reactor curve. However, the

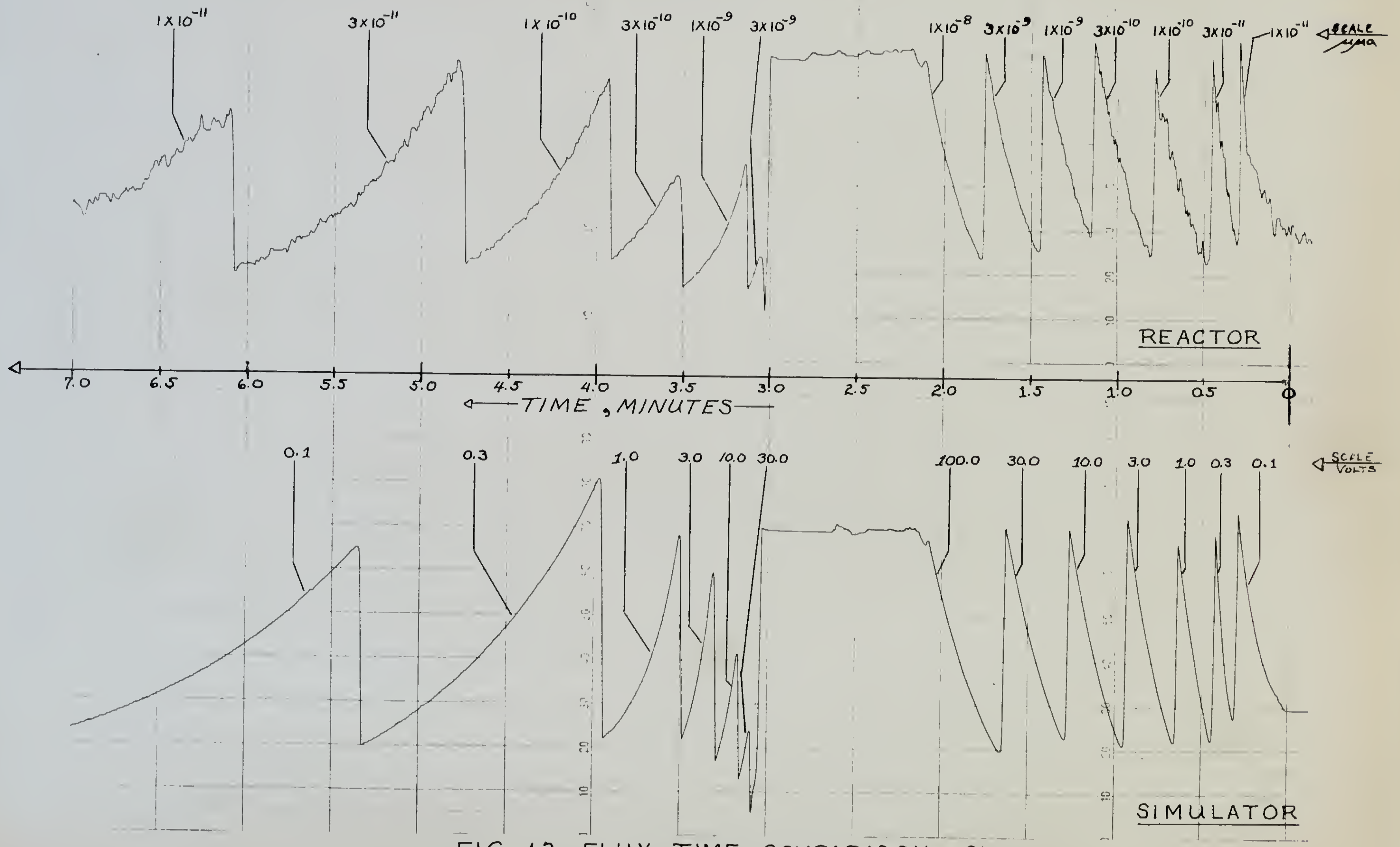

FIG. 13. FLUX-TIME COMPARISON CURVES

general nature of the two decay schemes is quite similar with the flux levels of reactor and simulator being 3.4×10^3 and 2.3×10^3 respectively four minutes after scramming.

The sequence of events describing Figure 14 is given in Table 5.

TABLE 5. SEQUENCE OF EVENTS FOR FIGURE 14

TIME IN MINUTES	REACTOR SEQUENCE	CORRESPONDING SIMULATOR SEQUENCE
—	Approximately steady flux level; rods@ 20.0 cm; glory hole empty; temp. 21 °C.	Steady flux level rods @ 22.0 cm; MRCTC potentiometer set for proper max. react. conditions.
0	Quickly inserted all poly, graphite, and lead discs into glory hole to provide a step change from about (-) 1300 $\mu\rho$ to (+) 1300 $\mu\rho$ conditions. Permitted flux to increase to about 0.73×10^6.	Quickly rotated MRCTC potentiometer to simulate step change of about 2600 $\mu\rho$ bringing simulator from a subcritical condition of about (-) 1300 $\mu\rho$ to a supercritical condition of about (+) 1300 $\mu\rho$. Permitted flux level to increase to about 0.73×10^6.
2.5	Quickly removed all poly to provide step change from a supercritical condition of about (+) 1300 $\mu\rho$ to a subcritical condition of about (-) 1300 $\mu\rho$.	Quickly rotated MRCTC potentiometer back to original setting corresponding to a step change in reactivity from about (+) 1300 $\mu\rho$ to about (-) 1300 $\mu\rho$.

The current output in $\mu\mu$ amps. from an ion chamber feeds the linear recorder on the reactor; the appropriate scales are labeled in the three figures. Corresponding to these are the voltage scales on the simulator which are also labeled in the figures. For example, the 1×10^{-8} $\mu\mu a$ scale on the reactor corresponds to the 100 volt scale on the simulator, the 1×10^{-9} $\mu\mu a$ corresponds to the 10 volt scale, the 1×10^{-10} $\mu\mu a$

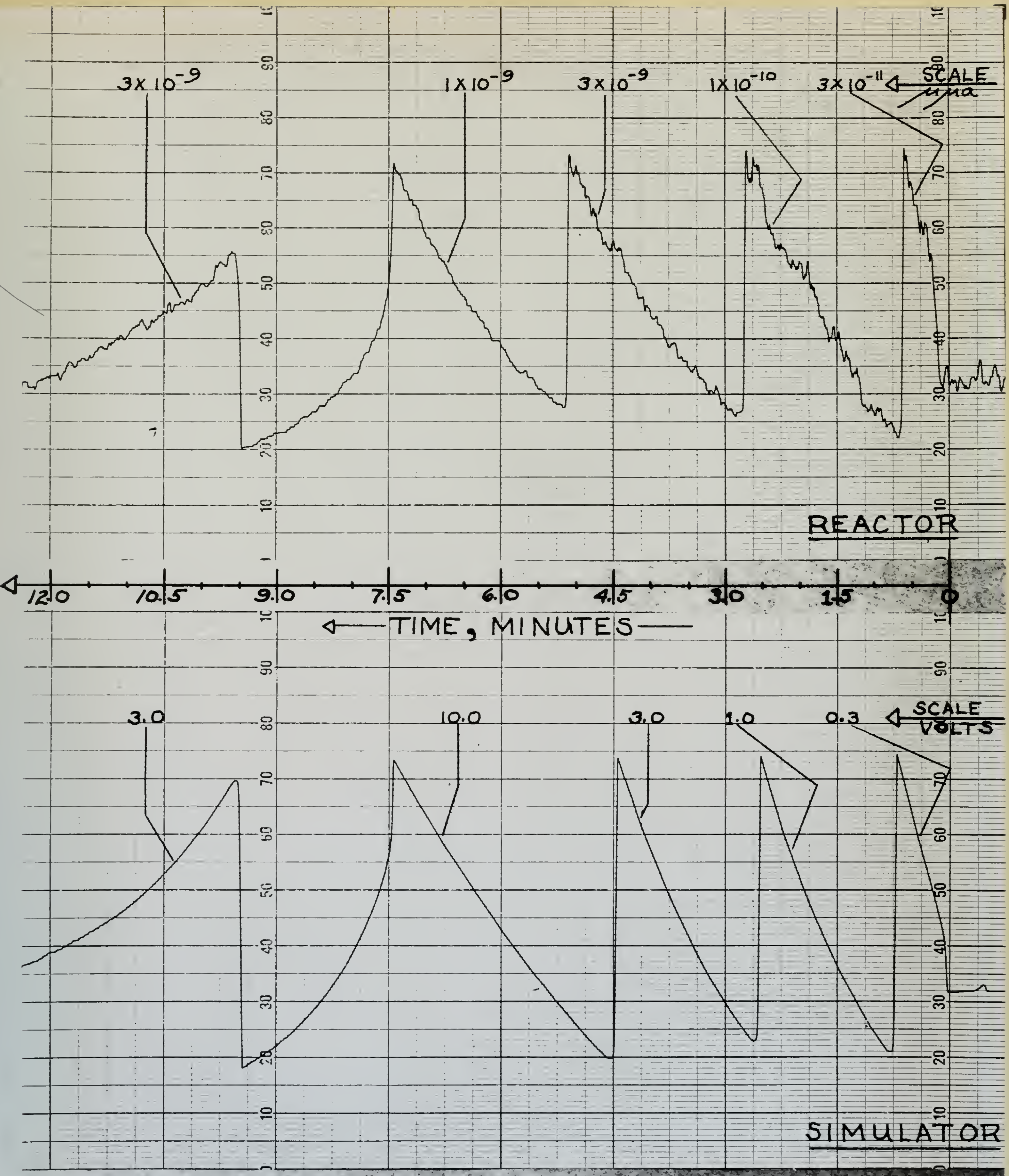

FIG. 14. FLUX-TIME COMPARISON CURVES

to the 1 volt scale, and the 1 x 10^{-11} $\mu\mu$a to the 0.1 volt scale. The reading in $\mu\mu$a as well as the reading in volts, of course, are proportional to a certain flux level. The flux level at the center of the core at a power level of 100 mw is given as 4.5 x 10^6. This corresponds to a 0.45 x 10^{-8} $\mu\mu$a output from the ion chamber or a 45 volt output from the simulator; all other values are scaled accordingly.

7. Conclusions

As evidenced by the comparison curves of Figures 12 through 14, reasonably accurate simulation of the time dependent behavior of a specific low power thermal reactor may be readily accomplished despite the many simplifying assumptions made in the development and electrical duplication of the governing transient equations. The final simulator with its relatively simple control system provides a useful tool with which to observe typical reactor responses resulting from the many sequences of operations to which a reactor of this type might be subject.

BIBLIOGRAPHY

1. S. Glasstone and M. Edlund, The Elements of Nuclear Reactor Theory, D. Van Nostrand Co., 1952
2. S. Glasstone, Principles of Nuclear Reactor Engineering, D. Van Nostrand Co., 1955
3. R. L. Murray, Nuclear Reactor Physics, Prentice Hall, Inc., 1957
4. M. A. Schultz, Control of Nuclear Reactors and Power Plants, McGraw-Hill Book Company, 1955
5. W. Pagels, A Portable Electronic Pile Kinetic Simulator AIEE Trans., Vol. 70, paper 51-262, 1951
6. K. H. Fishbeck, Nuclear Reactor Simulators, Convention Record IRE 1954 National Convention, pt. 9, Medical and Nuclear Electronics, IRE, 1954
7. F. E. O'Meara, Reactor Simulators, Journal of Applied Physics, Vol. 24, No. 9, September 1953
8. R. C. H. Wheeler, Basic Theory of the Electronic Analog Computer, Donner Scientific Company, California, 1957
9. A. T. Biehl, R. Fayram, et al, The AGN 201, A Safe, Low Power, Portable, Nuclear Reactor, Aerojet-General Nucleonics, San Ramon, California, August 1956.
10. M. M. Harvey, G. A. Linenberger, R. E. Nather, J. D. Randall, H. G. Simens, A Summary of Experimental Investigations of the AGN-201, Aerojet-General Nucleonics, San Ramon, California, June 10, 1957.

APPENDIX

CIRCUIT ANALYSIS DETERMINATION OF CURRENT I_8

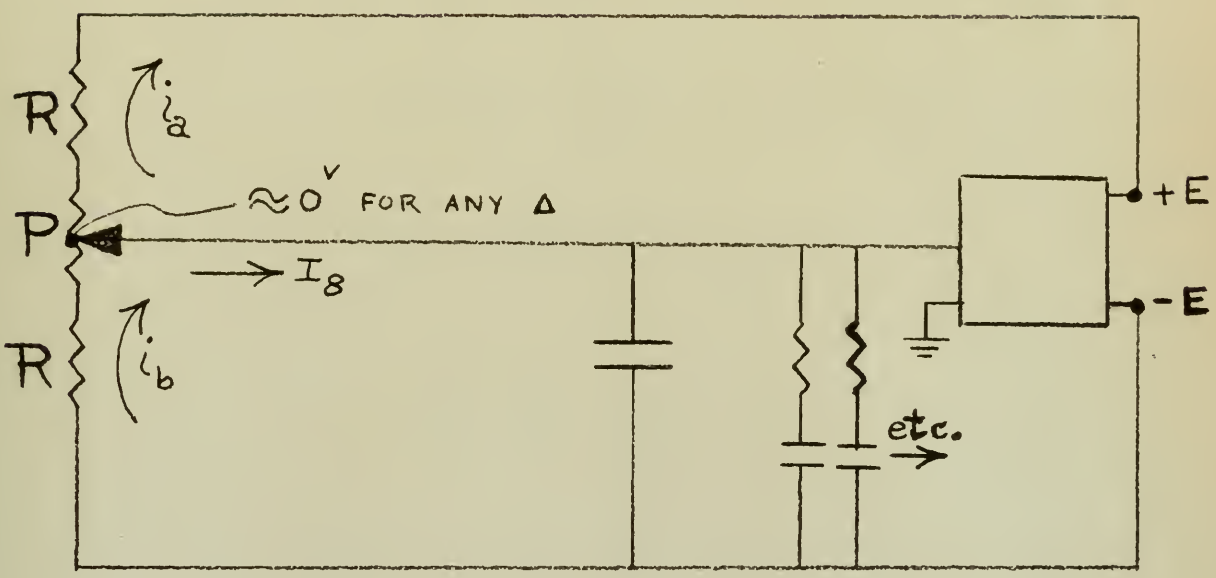

Assume current directions as indicated. Therefore,

$$i_b - i_a = I_8$$

Now, let Δ = proportional distance of P from mid or zero position.

Then

$$i_b = \frac{-E - 0}{R + P/2 \quad (1 + \Delta)}$$

$$i_a = \frac{0 - E}{R + P/2 \quad (1 - \Delta)}$$

Therefore,

$$I_8 = \frac{-E}{R + P/2 \quad (1 + \Delta)} + \frac{E}{R + P/2 \quad (1 - \Delta)}$$

or $$I_g = E \left[\frac{1}{R + P/2\ (1 - \Delta)} - \frac{1}{R + P/2\ (1 + \Delta)} \right]$$

$$= E \left[\frac{2\,\Delta\,P/2}{\left\{R + P/2\ (1 - \Delta)\right\} \left\{R + P/2\ (1 + \Delta)\right\}} \right]$$

$$= \frac{E\,\Delta\,P}{R^2 + \frac{RP}{2} \left[(1 + \Delta) + (1 - \Delta)\right] + \frac{P^2}{4} (1 - \Delta^2)}$$

$$I_g = \frac{\Delta\,E}{\frac{R^2}{P} + R + \frac{P}{4}\ (1 - \Delta^2)}$$

or $$I_g = \frac{\Delta\,E}{R \left[(1 + \frac{R}{P}) + \frac{P}{4R}\ (1 - \Delta^2)\right]}$$

APPENDIX II

SCALING FACTOR CALCULATIONS

Referring to scaling factor equation, namely

$$\left\{\frac{\zeta c_7}{l_o^*}\right\} = \left\{\frac{\zeta}{R(1 + R/P)\rho_{max}}\right\} = \left\{\frac{\zeta}{\beta_1 R_1}\right\} = \left\{\frac{V}{R_9 S_{o\,(max)}\ l_o^*}\right\} \tag{22}$$

let R_9 = 10 Megohms. This is an arbitrary value and is purposely chosen large to permit reasonable values of voltage V which is dependent on the very short neutron lifetime of this reactor.

Next, assume a value of neutron lifetime l^* of 10^{-4} sec. Since the reactor will not be far from critical at any time, l^* and l_o^* will be essentially equal to each other. Hence, as a first approximation l_o^* will also be assigned a value of 10^{-4} sec.

Now from control rod calibration data, ρ_{max} can be determined. In view of the fact that normal operating temperatures are about 23°C, ρ_{max} will be determined at this temperature assuming a homogeneous core (i.e., moderator, reflector, and shielding material in the glory hole). The operating range of reactivity here is

$$(-)\ .034775 \text{ to } (+)\ .004550$$

Therefore, ρ_{max} can be taken as .034775; and an imposed unbalance in the resistance values of R will prevent any positive reactivity value greater than .004550. In other words, when Δ is (-) 1, $\rho = -\rho_{(max)}$

A relationship must now be established between voltage E and neutron population density n. From known data,

ϕ at 100 mw = 4.5×10^6 neuts/cm²/sec

and $v = 1.28 \times 10^4 \sqrt{T^\circ K}$ cm/sec

or $v = 2.22 \times 10^5$ cm/sec at 23°C.

Therefore, $n = \dfrac{\phi}{v} = \dfrac{4.5 \times 10^6}{2.22 \times 10^5} = 20.25$ neuts/cm³

at rated power level, 100 mw.

Because the maximum output of the amplifier is 100 volts and because it might be desirable to directly correlate flux with observed voltage, 45 volts is made to correspond to 4.5×10^6 neutrons per cm² per sec. The constant of proportionality $\mathcal{J}$ is then given by

$$\mathcal{J} = \frac{E}{n} = \frac{45}{20.25} = 2.22$$

Next, a suitable value of potentiometer resistance P is selected so that after modifications by an external resistance to a center tap connection, a reasonable value of total resistance is still available. A 20K pot meets this requirement; and after modification as indicated in Figure 5, an overall resistance of 13.33K results (13.0K measured). It is to be noted that this value is not that which is to be substituted for P in equation (22). A P_{eff} must be determined which will be compatible with the derivation of the reactivity potentiometer relationships given in section 4. As far as the circuit is concerned, for zero or critical setting of the potentiometer the resistances on each side must be balanced. Therefore, since a (-) .034775 reactivity is required on one side, or in terms of resistance

$$\left(\frac{.034775}{.034775 + .00455}\right) \cdot 13K = (.885) \cdot (13) = 11.5 \text{ K}\Omega$$

This implies a value of

$$P_{eff} = 2 \times 11.5\ K\Omega = 23.0\ K\Omega$$

which should then be utilized in (22) in place of P. Now, because the actual resistance of P is only 13.0 K, then 10K additional resistance is required in loop 2 as indicated in Figure 6, or $R_2 = R_1 + 10K\Omega$. Values of β_1 are readily available and are given in the summary of scaling factor values at the end of section 5. Before calculations begin, a value of R must also be selected. First, however, since it is on this resistance that the individual values in the six Rc networks will depend, investigation to ensure reasonable magnitudes for the Rc delay networks is necessary. Based upon this investigation, a final value of R = 119K yields suitable magnitudes for all six delay components. Therefore, $R_1 = 119K$ and $R_2 = 119K + 10K = 129\ K\Omega$. It is also noted here that $R \approx 5P$ which yields better than 1% linearity between ρ and Δ. Calculations can now proceed as follows:

$$R(1 + R/P)\rho_{max} = 119 \times 10^3 \left(1 + \frac{119}{23}\right) 0.034775$$

$$= 2.55 \times 10^4\ \Omega$$

Now, from (22)

$$\frac{\zeta c_7}{l_0^*} = \frac{\zeta}{R(1 + R/P)\rho_{max}}$$

$$\text{or} \quad c_7 = \frac{l_o^*}{R(1 + R/P)\rho_{max}} = \frac{10^{-4}}{2.55 \times 10^4}$$

$$c_7 = .00392 \ \mu f$$

Likewise,

$$\frac{\zeta}{R\ (1 + R/P)\rho_{max}} = \frac{\zeta}{\beta_i\ R_i}$$

$$\text{or} \qquad = \frac{R\ (1 + R/P)\rho_{max}}{\beta_i} = \frac{2.55 \times 10^4}{\beta_i}$$

i	β_i	λ_i sec^{-1}	R_i megs	c_i μf
1	.00025	14	102	0.0007
2	.00085	1.61	30	0.0207
3	.00241	0.455	10.6	0.208
4	.00213	0.154	12.0	0.544
5	.00166	0.0315	15.4	2.06
6	.00025	0.0125	102	0.785

$$\beta = \sum_{i=1}^{6} \beta_i = .00755$$

Next, the method for deciding upon a suitable value of source voltage, V, as discussed in section 5, is as follows:

$$S_o = \frac{n(1-K_{eff})}{l^*} = \frac{-\rho n}{l_o^*}$$

Now, $n_{@30\ \mu w}$ = Power ratio x $n_{@100mw}$

$$= \frac{30 \times 10^{-6}}{100 \times 10^{-3}} \times 20.25$$

or $n_{@30\ \mu w} = 6.08 \times 10^{-3}$ neuts / cm^3 / sec

$\rho = \frac{K_{eff} - 1}{K_{eff}}$ @ safeties up position = (-) .009625

from control rod calibration data. From this then,

$$K_{eff} = .99047$$

$$\text{or } (1-K_{eff}) = .00953$$

Therefore,

$$S_o l^* = .579 \times 10^{-4}$$

$$\text{and} \quad S_o l_o^* = .585 \times 10^{-4}$$

Therefore,

$$V = \frac{\zeta R_9 \left(S_{o\,(max)}\ l_o^*\right)}{R\ (1 + R/P)\rho_{max}}$$

or

$$V = \frac{(2.22)\cdot(10 \times 10^{6})\cdot(.585 \times 10^{-4})}{(2.55 \times 10^{4})}$$

$$V = 51.0 \quad mv$$

It is to be noted that, in the case of the simulation of the AGN-201, S_o and $S_{o\,(max)}$ are the same since it is not desired to vary the source

strength (voltage); and therefore only the one magnitude determined above is needed to represent the effectively constant Ra-Be neutron source in the reactor.

Finally, if l^* is taken as 10^{-4} sec, then the value of S_0 is readily found to be

$$S_0 = \frac{.579 \times 10^{-4}}{10^{-4}} = .579 \text{ neuts/cm}^3\text{/sec}$$

MR 20 58
MR 20 58 620

Due April 20'58
E N Fennessey
ONR. 1000 Geary
San Francisco, Calif.

Thesis
W234 Watkins 36696
A low power reactor
simulator.

FE 26 58 BINDERY
MR 20 58
MR 20 58 E N Fennessey 620
JL 10 58 1138

The
W2

Thesis 36696
W234 Watkins
A low power reactor simulator

thesW234
A low range power reactor simulator.
3 2768 001 93004 3
DUDLEY KNOX LIBRARY